Title Page:

Spatial and temporal pattern of structure-function coupling of human brain connectome with development

Guozheng Feng[1,2,3], Yiwen Wang[1,2,3], Weijie Huang[1,2,3], Haojie Chen[1,2,3], Jian Cheng[4], Ni Shu[1,2,3,*]

[1]State Key Laboratory of Cognitive Neuroscience and Learning & IDG/McGovern Institute for Brain Research, Beijing Normal University, Beijing, China;

[2]BABRI Centre, Beijing Normal University, Beijing, China;

[3]Beijing Key Laboratory of Brain Imaging and Connectomics, Beijing Normal University, Beijing, China;

[4]School of Computer Science and Engineering, Beihang University, Beijing, China;

[*]Corresponding To:

Ni Shu, PhD, State Key Laboratory of Cognitive Neuroscience and Learning & IDG/McGovern Institute for Brain Research, Beijing Normal University, Beijing 100875, China; Tel: +86 10 58806154; Fax: +86 10 58806154; E-mail: nshu@bnu.edu.cn.

Abstract

Brain structural circuitry shapes a richly patterned functional synchronization, supporting for complex cognitive and behavioural abilities. However, how coupling of structural connectome (SC) and functional connectome (FC) develops and its relationships with cognitive functions and transcriptomic architecture remain unclear. We used multimodal magnetic resonance imaging data from 439 participants aged 5.7 to 21.9 years to predict functional connectivity by incorporating intracortical and extracortical structural connectivity, characterizing SC-FC coupling. Our findings revealed that SC-FC coupling was strongest in the visual and somatomotor networks, consistent with evolutionary expansion, myelin content, and functional principal gradient. As development progressed, SC-FC coupling exhibited heterogeneous alterations dominated by an increase in cortical regions, broadly distributed across the somatomotor, frontoparietal, dorsal attention, and default mode networks. Moreover, we discovered that SC-FC coupling significantly predicted individual variability in general intelligence, mainly influencing frontoparietal and default mode networks. Finally, our results demonstrated that the heterogeneous development of SC-FC coupling is positively associated with genes in oligodendrocyte-related pathways and negatively associated with astrocyte-related genes. This study offers insight into the maturational principles of SC-FC coupling in typical development and developmental disorders.

Keywords: structure-function coupling, brain connectome, development, cognitive function, gene transcriptome

Introduction

In neural circuitry, long-range (extracortical) interconnections among local (intracortical) microcircuits shape and constrain the large-scale functional organization of neural activity across the cortex[1-5]. The coupling of structural connectome (SC) and functional connectome (FC) varies greatly across different cortical regions reflecting anatomical and functional hierarchies[1, 6-9] as well as individual differences in cognitive function[8, 9], and is regulated by genes[6, 8]. Despite its fundamental importance, our understanding of the development of SC-FC coupling is currently limited. Specifically, the alterations in SC-FC coupling during development, its association with cognitive functions, and the underlying spatial transcriptomic mechanisms remain largely unknown.

Network modelling of the brain enables the characterization of complex information interactions at a system level and provides natural correspondences between structure and function in the cortex[7, 10]. Advances in diffusion MRI (dMRI) and tractography techniques have allowed the *in vivo* mapping of the white matter (WM) connectome (WMC), which depicts extracortical excitatory projections between regions[11]. The T1- to T2-weighted (T1w/T2w) ratio of MRI has been proposed as a means of quantifying microstructure profile covariance (MPC), which reflects intracortical microcircuit differentiation in molecular, cellular, and laminar differentiation[6, 12-15]. Resting state functional MRI (rs-fMRI) can be used to derive the FC, which captures the synchronization of neural activity[16]. A variety of statistical[6, 8, 9], communication[1, 7], and biophysical[5, 17] models have been proposed to study the SC-FC coupling. The communication model is particularly useful because it not only depicts indirect information transmission but also takes into account biodynamic information within acceptable computational complexity[7, 18]. However, most studies have relied on WMC-derived extracortical communications as SC to predict FC, while ignoring the intracortical microcircuits, the MPC. In the present study, we propose that incorporating both intracortical and extracortical SC provides a more comprehensive perspective for characterizing the development of SC-FC coupling.

Previous studies in adults have revealed that the SC-FC coupling is strongest in sensory cortex regions and weakest in association cortex regions, following the general functional and cytoarchitectonic hierarchies of cortical organization[1]. This organization may occur due to structural constraints, wherein cortical areas with lower myelination and weaker WM connectivity

tend to have more dynamic and complex functional connectivity[1, 8]. Large-scale association networks emerged over evolution by breaking away from the rigid developmental programming found in lower order sensory systems[19], facilitating regional and individual specialization[1,][20]. In terms of developmental changes in SC-FC coupling, a statistical model-based study[9] identified positive age-related changes in some regions, while fewer regions exhibited negative changes. Furthermore, there is evidence that SC-FC coupling is linked to cognitive functions in healthy children[21], adults[8, 22] and patients[23], suggesting that it may be a critical brain indicator that encodes individual cognitive differences. Nonetheless, a more comprehensive investigation is needed to understand the precise pattern of SC-FC coupling over development and its association with cognitive functions.

Cortical SC-FC coupling is highly heritable[8] and related to heritable connectivity profiles[6], suggesting that the development of coupling may be genetically regulated. The Allen Human Brain Atlas (AHBA)[24] is a valuable resource for identifying genes that co-vary with brain imaging phenotypes and for exploring potential functional pathways and cellular processes via enrichment analyses[25-27]. For instance, a myeloarchitectural study showed that enhanced myelin thickness in mid-to-deeper layers is specifically associated with the gene expression of oligodendrocytes[28]. Another functional study found that the expression levels of genes involved in calcium ion-regulated exocytosis and synaptic transmission are associated with the development of a differentiation gradient[29]. However, the transcriptomic architecture underlying the development of SC-FC coupling remains largely unknown.

In this study, we analysed data obtained from the Lifespan Human Connectome Project Development (HCP-D)[30], which enrolled healthy participants ranging in age from 5.7 to 21.9 years. Our main objective was to investigate the SC-FC coupling of brain connectome and characterize its developmental landscapes. Specifically, we aimed to determine whether the SC-FC coupling encodes individual differences in cognition during development. Finally, we explored the genetic and cellular mechanisms underlying the development of SC-FC coupling of brain connectome. To assess the reproducibility of our findings, sensitivity and replication analyses were performed with a different tractography algorithm and a split-half independent validation method.

Results

We selected 439 participants (5.7 – 21.9 years of age, 207 males) in the HCP-D dataset who met our inclusion criteria: available high-quality T1/T2, dMRI, and rs-fMRI data that met the quality control thresholds. For each participant, we generated multiple connectomes using 210 cortical regions from the Human Brainnetome Atlas (BNA)[31], which comprised MPC, WMC, and FC. Intracortical connectivity was represented by MPC. According to the WMC, twenty-seven weighted communication models[7] were calculated to characterize geometric, topological, or dynamic connectivity properties. Further details on these models can be found in Text S1. After analysis, we found that communicability[32], mean first passage times of random walkers[33], and flow graphs (timescales=1) provided the optimal combination of extracortical connectivity properties (p<0.05, 1,000 spin test permutations, Table S1).

Spatial pattern of cortical SC-FC coupling. We used SCs (MPC and three WMC communication models) to predict FC per node based on a multilinear model[1] (Figure 1), and quantified the nodewise SC-FC coupling as an adjusted coefficient of determination r^2. We observed that the grouped SC-FC coupling varied across cortical regions (mean adjusted r^2 = 0.14 ± 0.08, adjusted r^2 range = [0.03, 0.45], Figure 2A), and regions with significant coupling were located in the middle frontal gyrus, precentral gyrus, paracentral lobule, superior temporal gyrus, superior parietal lobule, postcentral gyrus, cingulate gyrus, and occipital lobe (p<0.05, 1,000 spin test permutations, Figure 2B). Similar heterogeneous patterns of coupling were observed when categorizing cortical regions into seven functional subnetworks[34] (visual, somatomotor, dorsal attention, ventral attention, limbic, frontoparietal and default mode networks). In the visual, somatomotor, default mode and ventral attention networks, SC significantly predict FC variance (p<0.05, 1,000 spin test permutations, Figure 2C). The visual and somatomotor networks had higher coupling values than the other networks (p<0.05, Kruskal-Wallis ANOVA, Figure 2C). We further investigated the alignment between SC-FC coupling and three fundamental properties of brain organization: evolution expansion[35], myelin content[36], and functional principal gradient[37]. Our findings reveal a negative association between regional distribution of SC-FC coupling and evolution expansion (Spearman's r=-0.52, p<0.001, 1,000 spin test permutations, Figure 2D), as well as with the functional principal gradient (Spearman's r=-0.46, p<0.001, 1,000 spin test

permutations, Figure 2F). Conversely, nodes exhibiting higher SC-FC coupling tended to exhibit higher myelin content (Spearman's r=0.49, p<0.001, 1,000 spin test permutations, Figure 2E).

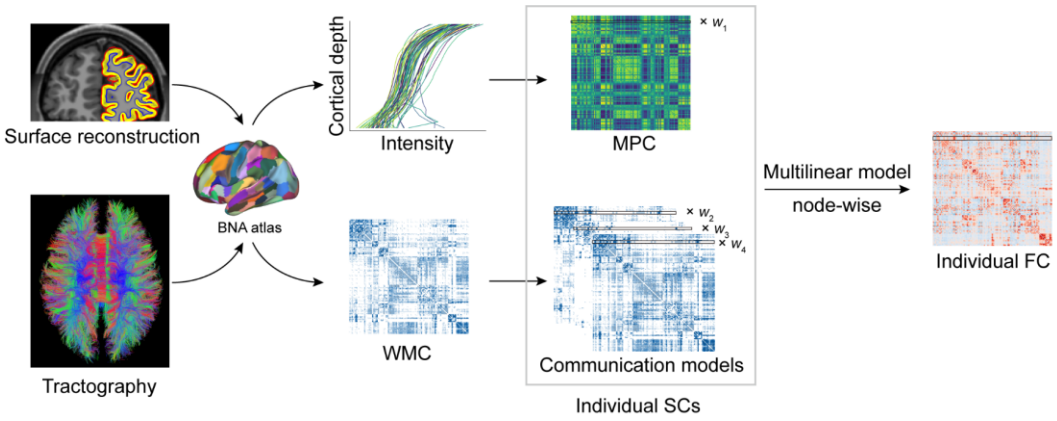

Figure 1. SC-FC coupling framework. The framework used to quantify nodal SC-FC coupling in the human brain. MPC was used to map networks of intracortical microstructural similarity for each cortical node. The WMC represents the extracortical excitatory projection structure, and communication models were then constructed to represent the complex process of communication. A multilinear model was constructed to examine the association of individual nodewise SC (MPC and communication models) profiles with FC profiles.

Additionally, we applied Haufe's inversion transform[38] to yield predictor weights of various SCs, where higher or lower values indicate stronger positive or negative correlations with FC. Our results demonstrated that different SCs had preferential contributions to FC variance across cortical regions to explain FC variance (p<0.05, FDR corrected, Kruskal-Wallis ANOVA, Figure 2G). Specifically, in the MPC, regions with positive correlation were the orbital gyrus, precentral gyrus, right middle temporal gyrus and temporoparietal junction, while regions with negative correlations were the left superior frontal gyrus, inferior parietal lobule and bilateral cingulate gyrus. Regarding WMC communication models, the communicability and flow graphs tended to stronger higher positive correlations in the visual, limbic and default mode networks, whereas the mean first passage time had stronger negative correlations in the somatomotor, limbic and frontoparietal networks.

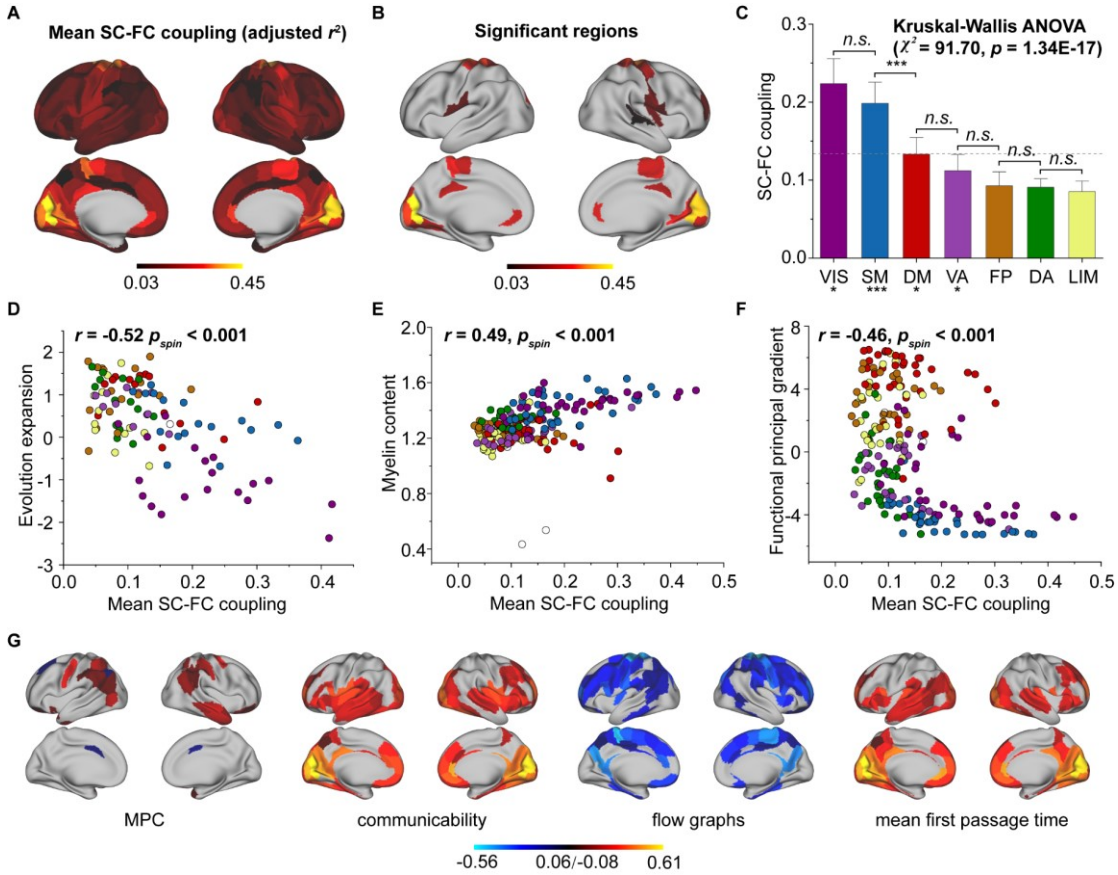

Figure 2. Cortical SC-FC coupling in young individuals. (A) Spatial pattern of SC-FC coupling. (B) Spatial patterns with significant predictions (p<0.05, spin test). (C) SC-FC coupling comparisons among functional networks. The error bars represent 95% confidence intervals. (D-F) SC-FC coupling aligns with evolution expansion, myelin content and functional principal gradient. (G) Preferential contributions of cortical regions across different structural connections. Note: ***: p<0.001; **: p<0.01; *: p<0.05; *n.s.*: p>0.05. VIS, visual network; SM, somatomotor network; DA, dorsal attention network; VA, ventral attention network; LIM, limbic network; FP, frontoparietal network; DM, default mode network.

Age-related changes in SC-FC coupling with development. To track changes in SC-FC coupling during development, we used a general linear model to assess the effect of age on nodal SC-FC coupling, while controlling for sex, intracranial volume, and in-scanner head motion. Our results revealed that the whole-cortex average coupling increased during development (β_{age}=1.05E-03, F=3.76, p=1.93E-04, r=0.20, p=3.20E-05, Figure 3A). Regionally, the SC-FC coupling of most cortical regions increased with age (p<0.05, FDR corrected, Figure 3B), particularly that in the frontal lobe, middle temporal gyrus, inferior temporal gyrus, parietal lobe, cingulate gyrus and

lateral occipital cortex. Conversely, cortical regions with significantly decreased SC-FC coupling (p<0.05, FDR corrected, Figure 3B) were located in left orbital gyrus, left precentral gyrus, right superior and inferior temporal gyrus, left fusiform gyrus, left superior parietal lobule, left postcentral gyrus, insular gyrus, and cingulate gyrus. Regarding functional subnetworks, SC-FC coupling increased disproportionately with age (Figure 3C), wherein the somatomotor (β_{age}=2.39E-03, F=4.73, p=3.10E-06, r=0.25, p=1.67E-07, Figure 3E), dorsal attention (β_{age}=1.40E-03, F=4.63, p=4.86E-06, r=0.24, p=2.91E-07, Figure 3F), frontoparietal (β_{age}=2.11E-03, F=6.46, p=2.80E-10, r=0.33, p=1.64E-12, Figure 3I) and default mode (β_{age}=9.71E-04, F=2.90, p=3.94E-03, r=0.15, p=1.19E-03, Figure 3J) networks significantly increased with age and exhibited greater increased. No significant correlations were found between developmental changes in SC-FC coupling and the fundamental properties of cortical organization. Additionally, weights of different SCs varied with age, showing that MPC weight was positively correlated with age and that the weights of WMC communication models were stable (Figure S1-S4).

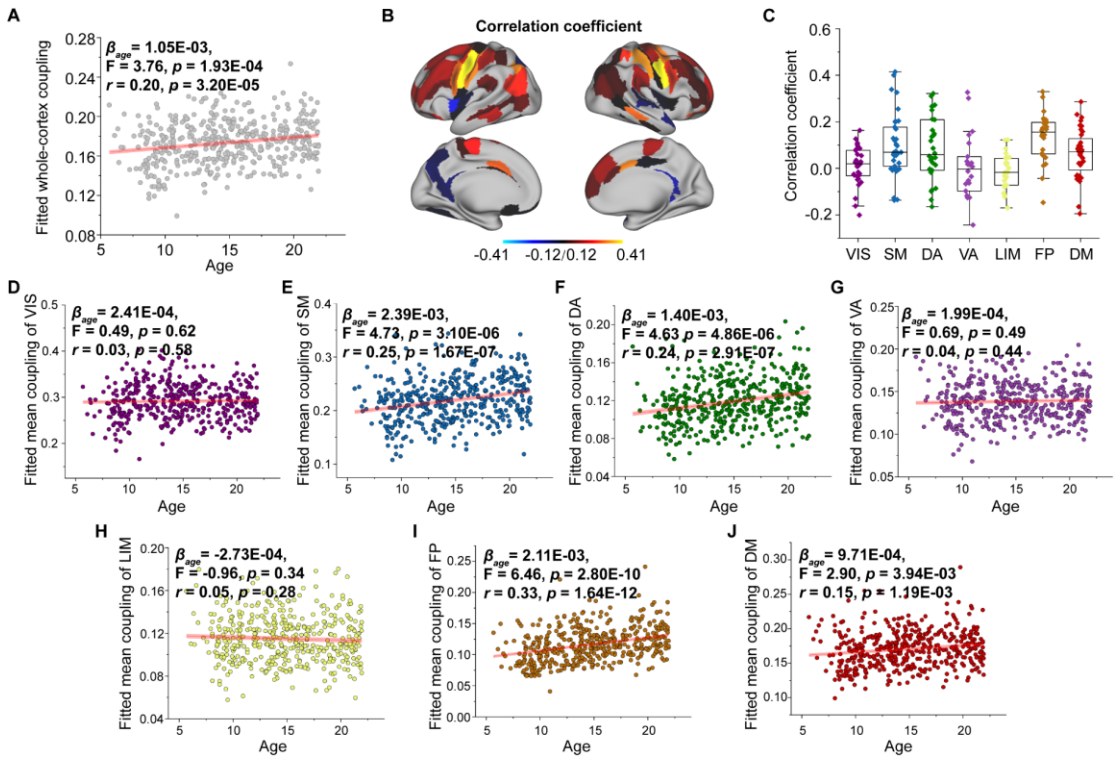

Figure 3. Aged-related changes in SC-FC coupling. (A) Increases in whole-brain coupling with age. (B) Correlation of age with SC-FC coupling across significant regions (p<0.05, FDR corrected). (C) Comparisons of age-related changes in SC-FC coupling among functional networks. The boxes

show the median and interquartile range (IQR; 25–75%), and the whiskers depict 1.5× IQR from the first or third quartile. (D-J) Correlation of age with SC-FC coupling across the VIS, SM, DA, VA, LIM, FP and DM. VIS, visual network; SM, somatomotor network; DA, dorsal attention network; VA, ventral attention network; LIM, limbic network; FP, frontoparietal network; DM, default mode network.

SC-FC coupling predicts individual differences in cognitive functions. As we found that SC-FC coupling can encode brain maturation, we next evaluated the implications of coupling for individual cognition using Elastic-Net algorithm[11]. After controlling for sex, intracranial volume and in-scanner head motion, we found the SC-FC coupling significantly predicted individual differences in fluid intelligence, crystal intelligence and general intelligence (Pearson's r=0.3~0.4, p<0.001, FDR corrected, Figure 4A), suggesting that increased SC-FC coupling during development is associated with higher intelligence. Furthermore, even after controlling for age, SC-FC coupling remained a significant predictor of general intelligence (Pearson's r=0.11, p=0.01, FDR corrected, Figure 4A). The predictive performances for other cognitive subscores are shown in Figure S5. To identify the regions with the greatest contributions to individual differences in age-adjusted general intelligence, we utilized Haufe's inversion transform[38] to extract predictor weights across various regions. Our analysis revealed that SC-FC coupling within the prefrontal lobe, temporal lobe and lateral occipital lobe was the most predictive of individual differences in general intelligence (Figure 4B). In addition, we found that the frontoparietal and default mode networks were significantly predicted the general intelligence (p<0.01, 1,000 spin test permutations, Figure 4C).

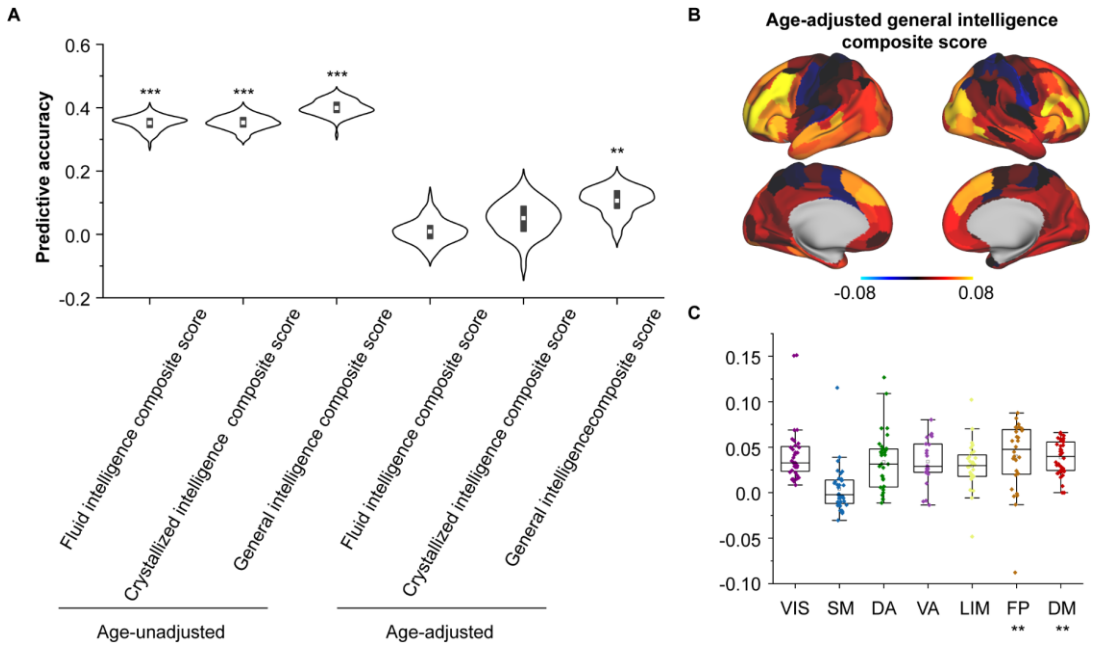

Figure 4. Encoding individual differences in intelligence using regional SC-FC coupling. (A) Predictive accuracy of fluid, crystallized, and general intelligence composite scores. (B) Distribution of brain regions contributing to the general intelligence composite score. (C) Predictive contribution of functional networks. The boxes show the median and interquartile range (IQR; 25–75%), and the whiskers depict the 1.5× IQR from the first or third quartile.

Transcriptomic and cellular architectures of SC-FC coupling development. We employed partial least square (PLS) analysis[39] to establish a link between the spatial pattern of SC-FC coupling development and gene transcriptomic profiles (Figure 5A) obtained from the AHBA using a recommended pipeline[40]. The gene expression score of the first PLS component (PLS1) explained the most spatial variance, at 22.26%. After correcting for spatial autocorrelation[41], we found a positive correlation (Pearson's r=0.41, p=0.006, 10,000 spin test permutations, Figure 5B) between the PLS1 score of genes and the spatial pattern of SC-FC coupling development. In addition, we identified potential transcriptomic architectures using a Gene Ontology (GO) enrichment analysis of biological processes and pathway[42], analysing the significant positive and negative genes in PLS1. The positive weight genes (364 genes) were prominently enriched for "myelination", "monoatomic cation transport", "supramolecular fiber organization", etc (p<0.05, FDR corrected, Figure 5C). The negative correlation genes (456 genes) were relatively weakly enriched in "cellular macromolecule biosynthetic process" and other pathways (p<0.05, FDR corrected, Figure 5C).

To further investigate cell-specific expression patterns associated with SC-FC coupling development, the selected genes in the AHBA were agglomerated into seven canonical cell classes[43-48]: astrocytes, endothelial cells, excitatory neurons, inhibitory neurons, microglia, oligodendrocytes and oligodendrocyte precursors (OPCs). Our findings showed that the genes with positive weights were significantly expressed in oligodendrocytes (75 genes, $p<0.001$, permutation test, Figure 5D). The genes with negative weights were expressed in astrocytes (43 genes, $p<0.001$, permutation test, Figure 5D). Additionally, genes enriched in positive pathways were intensively overexpressed in oligodendrocytes, while genes enriched in three negative pathways were expressed in astrocytes, inhibitory neurons and microglia ($p<0.05$, permutation test, Figure S6).

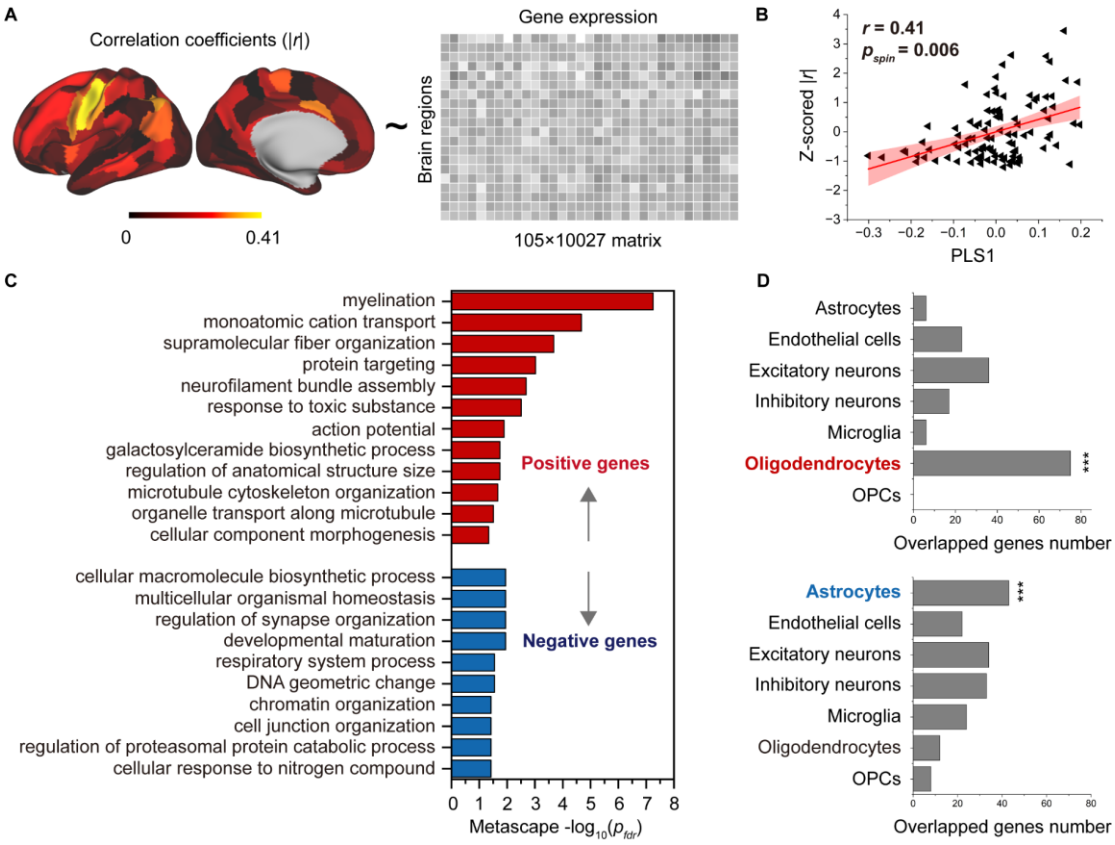

Figure 5. Association between developmental changes in SC-FC coupling and gene transcriptional profiles. (A) The map of developmental changes (absolute value of correlation coefficients) in SC-FC coupling across 105 left brain regions (left panel), and the normalized gene transcriptional profiles containing 10,027 genes in 105 left brain regions (right panel). (B) The correlation between developmental changes in SC-FC coupling and the first PLS component from the PLS regression analysis. (C) Enriched terms of significant genes. (D) Cell type-specific

expression of significant genes. Note, p_{spin}: spin test; p_{fdr}: FDR corrected.

Reproducibility analyses. *Different parcellation templates.* To evaluate the robustness of our findings to different parcellation templates, using the multimodal parcellation from the Human Connectome Project (HCPMMP)[49], we repeated the analyses of the cortical patterns of SC-FC coupling and correlation of age with SC-FC coupling. We observed a similar distribution in SC-FC coupling in which visual and somatomotor networks had higher coupling values than other networks (Figure S7A). The SC-FC coupling of most cortical regions increased with age (Figure S7B), and the significant regions were similar to those in the main findings (Figure S7C, $p<0.05$, FDR corrected).

Different tractography strategies. To evaluate the sensitivity of our results to tractography strategies, we reconstructed fibres using deterministic tractography with a ball-and-stick model and generated a fibre number-weighted network for each participant. This same pipeline was employed for subsequent SC-FC coupling, prediction, and gene analyses. These two tractography strategies yielded similar findings, as indicated by significant correlations in the mean SC-FC coupling ($r=0.85$, $p<0.001$, spin test, Figure S8A), the correlation of between age and SC-FC coupling ($r=0.79$, $p<0.001$, spin test, Figure S8B), predictive weights on the general intelligence ($r=0.85$, $p<0.001$, spin test, Figure S8C), and gene weights ($r=0.80$, $p<0.001$, Figure S8D).

Split-half validation. To assess the reproducibility of our findings, we performed a split-half independent validation using the whole dataset (WD). Specifically, we randomly partitioned WD into two independent subsets (S1 and S2), and this process was repeated 1,000 times to mitigate any potential bias due to data partitioning. We then quantified SC-FC coupling, correlation between age and SC-FC coupling, and gene weights in S1 and S2 using the same procedures. Remarkably, we observed high levels of agreement among the datasets (S1, S2, and the WD) as demonstrated in Figure S9.

Discussion

In the present study, we characterized alterations of SC-FC coupling of brain connectome during development by combining intracortical and extracortical SC to predict FC based on the HCP-D dataset. We observed that SC-FC coupling was stronger in the visual and somatomotor networks

than in other networks, and followed fundamental properties of cortical organization. With development, SC-FC coupling exhibited heterogeneous changes in cortical regions, with significant increases in the somatomotor, frontoparietal, dorsal attention and default mode networks. Furthermore, we found that SC-FC coupling can predict individual differences in general intelligence, mainly with the frontoparietal and default mode networks contributing higher weights. Finally, we demonstrated that the spatial heterogeneity of changes in SC-FC coupling with age was associated with transcriptomic architectures, with genes with positive weights enriched in oligodendrocyte-related pathways and genes with negative weights expressed in astrocytes. Together, these findings characterized the spatial and temporal pattern of SC-FC coupling of brain connectome during development and the heterogeneity in the development of SC-FC coupling is associated with individual differences in intelligence and transcriptomic architecture.

Intracortical microcircuits are interconnected through extracortical WM connections, which give rise to richly patterned functional networks[1, 3]. Despite extensive research on this topic, the relationship between SC and FC remains unclear. Although many studies have attempted to directly correlate FC with the WMC, this correspondence is far from perfect due to the presence of polysynaptic (indirect) structural connections and circuit-level modulation of neural signals[2, 9, 16, 50]. Biological models can realistically generate these complex structural interconnections, but they have significant temporal and spatial complexity when solving for model parameters[51-54]. Communication models using the WMC integrate the advantages of different communication strategies and are easy to construct[18]. As there are numerous communication models, we identified an optimal combination consisting of three decentralized communication models based on predictive significance: communicability, mean first passage times of random walkers and flow graphs. We excluded a centralized model (shortest paths), which was not biologically plausible since it requires global knowledge of the shortest path structure[7, 55, 56]. In our study, we excluded the Euclidean distance and geodesic distance because spatial autocorrelation is inhibited. This study provides a complementary perspective (in addition to the role of WMC in shaping FC) that emphasizes the importance of intrinsic properties within intracortical circuit in shaping the large-scale functional organization of the human cortex. MPC can link intracortical circuits variance at specific cortical depths from a graph-theoretical perspective, enabling reflection of intracortical

microcircuit differentiation at molecular, cellular, and laminar levels[6, 12-15]. Coupling models that incorporate these microarchitectural properties yield more accurate predictions of FC from SC[3, 57].

SC–FC coupling may reflect anatomical and functional hierarchies. SC-FC coupling in association areas, which have lower structural connectivity, was lower than that in sensory areas. This configuration effectively releases the association cortex from strong structural constraints imposed by early activity cascades, promoting higher cognitive functions that transcend simple sensori-motor exchanges[19]. A macroscale functional principal gradient[37, 58] in the human brain has been shown to align with anatomical hierarchies. Our study revealed a similar pattern, where SC-FC coupling was positively associated with evolutionary expansion and myelin content, and negatively associated with functional principal gradient during development. These findings are consistent with previous studies on WMC-FC coupling[9] and MPC-FC coupling[6]. Notably, we also found that the coupling pattern differed from that in adults, as illustrated by the moderate coupling of the sensorimotor network in the adult population[8]. SC-FC coupling is dynamic and changes throughout the lifespan[7], particularly during adolescence[6, 9], suggesting that perfect SC-FC coupling may be unlikely. Moreover, our results suggested that regional preferential contributions across different SCs lead to variations in the underlying communication process. Interestingly, the two extremes of regions in terms of MPC correlations corresponded to the two anchor points of the gradient[28]. The preferential regions in WM communication models were consistent with the adult results[7].

In addition, we observed developmental changes in SC-FC coupling dominated by a positive increase in cortical regions[9], broadly distributed across somatomotor, frontoparietal, dorsal attention, and default mode networks[9]. In a lifespan study, the global SC-FC coupling alterations with age were driven by reduced coupling in the sensorimotor network[7]. This finding is consistent across age ranges, indicating that sensorimotor coupling changes appear throughout development and ageing. Furthermore, we investigated the relationships of coupling alterations with evolutionary expansion and functional principal gradient but found no significant correlations, in contrast to a previous study[9]. These discrepancies likely arise from differences in coupling methods, highlighting the complementarity of our methods with existing findings.

The neural circuits in the human brain support a wide repertoire of human behaviour[59]. Our study demonstrates that the degree of SC-FC coupling in cortical regions can significantly predict cognitive scores across various domains, suggesting that it serves as a sensitive indicator of brain maturity. Moreover, even after controlling for age effects, SC-FC coupling significantly predicted general intelligence, suggesting that it can partly explain individual differences in intelligence, as shown in previous studies[8]. In another study[9], positive correlations between executive function and SC-FC coupling were mainly observed in the rostro-lateral frontal and medial occipital regions, whereas negative associations were found in only the right primary motor cortex. While SC-FC coupling was not found to predict age-adjusted executive function in our study, we observed that the frontoparietal network and the default mode network specifically contributed higher positive prediction weights for general intelligence, whereas the somatomotor network had negative prediction weights[8]. The maturation of the frontoparietal network and default mode network continues into early adulthood, providing an extended window for the activity-dependent reconstruction of distributed neural circuits in the cross-modal association cortex[19]. As we observed increasing coupling in these networks, this may have contributed to the improvements in general intelligence, highlighting the flexible and integrated role of these networks.

Classic twin studies have reported that the heritability of coupling differs among cortical regions, with higher heritability in the visual network than in other cortical networks[8]. An inverse correlation between the pattern of SC-FC coupling and heritable connectivity profiles has been reported[6]. This led us to hypothesize that the development of SC-FC coupling may be influenced by the expression patterns of the genetic transcriptome across various cell types with different spatial distributions. Our findings suggest that the spatial development of SC-FC coupling is associated with underlying transcriptome structure. Specifically, genes positively associated with the development of SC-FC coupling were enriched in oligodendrocyte-related pathways. Oligodendrocytes, specialized glial cells in the central nervous system, play a crucial role in myelination by producing myelin sheaths that enable saltatory conduction and provide metabolic support to axons[60]. Defects in myelination have been linked to developmental disorders[61]. This seems to indicate that significant alterations in SC-FC coupling during development may reflect neural plasticity, such as activity-dependent myelination of axons connecting functionally coupled

regions[62, 63]. Conversely, we found that genes negatively correlated with SC-FC coupling were enriched in two specific gene pathways within astrocytes, inhibitory neurons and microglia. Both astrocytes and microglia have been implicated in synaptic pruning, a critical developmental process for the formation of fully functional neuronal circuits that eliminates weak and inappropriate synapses[64-66]. Importantly, the precise establishment of synapses is crucial for establishing the intercellular connectivity patterns of GABAergic neurons[67]. These findings suggest that the subtle alterations observed in SC-FC coupling are closely associated with the refinement of mature neural circuits.

Several methodological issues must be addressed. First, we implemented a conservative quality control procedure to address head motion, which unavoidably resulted in the loss of some valuable data. Given the confounding influence of head motion in fMRI studies, especially those involving developing populations, we applied censoring of high-motion frames and included motion as a covariate in the GLM analysis and cognitive prediction to minimize its effects[7, 59, 68, 69]. Second, although we observed SC-FC coupling across development by integrating intra- and extracortical SC to predict FC, it is worth noting that combining deep learning models[2], biophysical models[5, 17], or dynamic coupling[3, 13] perspectives may provide complementary insights. Third, we focused solely on cortico-cortical pathways, excluding subcortical nuclei from analysis. This decision stemmed from the difficulty of reconstructing the surface of subcortical regions[70] and characterizing their connections using MPC technique, as well as the challenge of accurately resolving the connections of small structures within subcortical regions using whole-brain diffusion imaging and tractography techniques[71, 72]. Fourth, it is important to acknowledge that changes in gene expression levels during development may introduce bias in the results, although a prior study[73] suggested that the relative spatial patterns of gene expressions remain stable after birth. Finally, validation of sensitivity across independent datasets is a crucial step in ensuring the reliability of our results. To address this, we employed an alternative split-half validation strategy and the results supported the reliability of the current findings. However, future verification of current findings on independent datasets are still needed.

Conclusions

Overall, this study sheds light on the development of SC-FC coupling in the brain and its relationship to cognitive function and gene expression patterns. The results improve our understanding of the fundamental principles of brain development and provide a basis for future research in this area. Further investigations are needed to fully explore the clinical implications of SC-FC coupling. Ultimately, this study has the potential to inform the development of novel interventions for a range of developmental disorders.

Materials and Methods

Participants. We selected 439 participants (207 males, mean age = 14.8 ± 4.2 years, age range = [5.7, 21.9]) from the HCP-D Release 2.0 data (https://www.humanconnectome.org/study/hcp-lifespan-development) after conducting rigorous checks for data completeness and quality control. The HCP-D dataset comprised 652 healthy participants who underwent multimodal MRI scans and cognitive assessments, and the detailed inclusion and exclusion criteria for this cohort have been described in[30]. All participants or their parents (for participants under the age of 18 years) provided written informed consent and assent. The study was approved by the Institutional Review Board of Washington University in St. Louis.

Imaging acquisition. The MRI data were obtained with a Siemens 3T Prisma with a 32-channel phased array head coil, and detailed imaging parameters are available in[74]. High-resolution T1w images were acquired using a 3D multiecho MPRAGE sequence (0.8 mm isotropic voxels, repetition time (TR)/inversion time (TI) = 2500/1000 ms, echo time (TE) = 1.8/3.6/5.4/7.2 ms, flip angle = 8°, up to 30 reacquired TRs). The structural T2w images were collected with a variable-flip-angle turbo-spin–echo 3D SPACE sequence (0.8 mm isotropic voxels, TR/TE = 3200/564 ms, up to 25 reacquired TRs). The dMRI scans included four consecutive runs with a 2D 4× multiband spin–echo echo-planar imaging (EPI) sequence (1.5 mm isotropic voxels, 185 diffusion directions with b = 1500/3000 s/mm^2 and 28 b = 0 s/mm^2 volumes, TR = 3.23 s, flip angle = 78°). The rs-fMR images were acquired using a 2D 8× multiband gradient-recalled echo EPI sequence (2.0 mm isotropic voxels, TR/TE = 800/37 ms, flip angle = 52°). Each rs-fMRI scan duration was 26 minutes (four runs of 6.5 minutes) for participants over 8 years old and 21 minutes (six runs of 3.5 minutes) for participants who were 5~7 years old.

Imaging preprocessing. All structural, diffusion and functional images underwent minimal preprocessing[70]. We specifically processed dMRI data referring to the publicly available code from https://github.com/Washington-University/HCPpipelines since the HCP-D has not released preprocessed dMRI results. Briefly, structural T1w and T2w images went through gradient distortion correction, alignment, bias field correction, registration to Montreal Neurological Institute (MNI) space, white matter and pial surface reconstruction, segment structures, and surface registration and downsampling to 32k_fs_LR mesh. A T1w/T2w ratio image, which indicates intracortical myelin, was produced for each participant[36]. Regarding fMRI data, the preprocessing pipeline included spatial distortion correction, motion correction, EPI distortion correction, registration to MNI space, intensity normalization, mapping volume time series to 32k_fs_LR mesh, and smoothing using a 2 mm average surface vertex. Following our previous methodological evaluation study[11], the dMRI procedures consisted of intensity normalization of the mean b0 image, correction of EPI distortion and eddy current, motion correction, gradient nonlinearity correction, and linear registration to T1w space.

Network computation. *Microstructure profile covariance (MPC).* The MPC can capture cytoarchitectural similarity between cortical areas[12]. We first reconstructed 14 cortical surfaces from the white matter to the pial surface using a robust equivolumetric model[12, 75]. Then, the T1w/T2w ratio image was used to sample intracortical myelin intensities at these surfaces. We aggregated the intensity profiles of vertices into 210 cortical regions according to the BNA[31]. Finally, we computed pairwise partial correlations between regional intensity profiles, while controlling for the average intensity profile. After removing negative correlations, we used Fisher's r-to-z-transformation to generate an individual MPC.

White matter connectome (WMC). Following our previous methodological evaluation study[11], the ball-and-stick model estimated from the bedpostx command-line in the FDT toolbox of FSL (https://fsl.fmrib.ox.ac.uk/fsl/fslwiki/FDT) was used to estimate fibre orientations (three fibres modelled per voxel)[76-79]. The BNA atlas was applied to individual volume space by inverse transformation derived from preprocessed steps. Next, probabilistic tractography[78, 80] was implemented in the FDT toolbox to estimate the probability of connectivity between two regions by sampling 5,000 fibres for each voxel within each region, correcting for distance, dividing

the total fibres number in source region, and calculating the average bidirectional probability[11]. Notably, the connections in subcortical areas were removed. A consistency-based thresholding approach (weight of the coefficient of variation at the 75th percentile) was used to remove spurious connections, and retain consistently reconstructed connections across subjects[9, 81]. Finally, twenty-seven communication models[7] were subsequently derived from the weighted probabilistic network, including shortest path length (gamma values = {0.12, 0.25, 0.5, 1, 2, 4}), communicability[32], cosine similarity, search information (weight-to-cost transformations = {0.12, 0.25, 0.5, 1, 2, 4})[82], path transitivity (weight-to-cost transformations = {0.12, 0.25, 0.5, 1, 2, 4})[55], matching index[83], greedy navigation[84], mean first passage times of random walkers[33], and flow graphs (timescales = {1, 2.5, 5, 10})[85]; for more details see Text S1.

Functional network (FC). To further clean the functional signal, we performed frame censoring, regressed out nuisance variables (including white matter, cerebrospinal fluid, global signal, and 12 motion parameters), and temporal bandpass filtering (0.01~0.1 Hz). Specifically, we identified censored frames with motion greater than 0.15[7] based on the Movement_RelativeRMS.txt file. We flagged one frame before and two frames after each censored frame, along with any uncensored segments of fewer than five contiguous frames, as censored frames as well[69]. We discarded fMRI runs with more than half of the frames flagged as censored frames, and excluded participants with fewer than 300 frames (less than 4 minutes). After censoring, regression of nuisance variables, and temporal bandpass filtering, we averaged the time series of vertices into 210 cortical regions according to the BNA[31]. We then computed pairwise Pearson's correlations between regional time series, and applied Fisher's r-to-z-transformation to the resulting correlations to generate individual FC.

SC-FC coupling. A multilinear model[1] was constructed to examine the relationship of individual nodewise SC profiles and FC profiles. For a given node, the predictive variable was nodal SC $\mathbf{S} = \{\boldsymbol{s}_1, \boldsymbol{s}_2, \cdots, \boldsymbol{s}_i, \cdots, \boldsymbol{s}_n\}$, $\boldsymbol{s}_i \in \mathrm{R}^m$ where $\boldsymbol{s}_i$ is the connectional profile of the ith modal, n is the number of structural modal, and m is the node number. The nodal functional profile $\boldsymbol{f}$ is the dependent variable.

$$\boldsymbol{f} = b_0 + b_1\boldsymbol{s}_1 + b_2\boldsymbol{s}_2 + \cdots + b_i\boldsymbol{s}_i + \cdots + b_n\boldsymbol{s}_n \quad (1)$$

where the intercept b_0 and regression coefficients b_i are estimated model parameters. For each

463 participant, goodness of fit per node represents the nodal coupling between SC and FC, quantified
464 as the adjusted coefficient of determination[7]

$$R^2_{adjusted} = 1 - \frac{(1 - R^2)(N_c - 1)}{N_c - N_p - 1} \quad (2)$$

465 where R^2 is the unadjusted coefficient of determination, N_c is the number of connection
466 excluding self-connections, and N_p is the number of predictors.

467 In the present study, WMC communication models that represented diverse geometric,
468 topological, or dynamic factors, were used to explain nodal FC variation. Notably, too many
469 predictors will result in overfitting and blindly increase the explained variance. To address this issue
470 and identify distinct communication mechanisms, we controlled for redundant predictors.
471 Specifically, we used all twenty-seven communication models to predict FC at the node level for
472 each participant. We applied Haufe's inversion transform[38] to obtain predictor weights for each
473 model, with higher or lower values indicating stronger positive or negative correlations with FC.
474 Next, we investigated the enrichment of the highest weights per region through a spin test[86] with
475 1,000 permutations to assess whether the number of highest weights across communication models
476 was significantly larger than that in a random discovery.

477 The significant communication models were used to represent WMC communication
478 properties and to predict functional profiles in conjunction with MPC as structural profiles
479 (predictors). To test the significance of the resulting adjusted R^2 values and system-specific of
480 coupling, we generated a null predictive model using a spin test[86] with 1,000 spatially-constrained
481 repetitions. We also used Kruskal-Wallis nonparametric one-way analysis of variance (Kruskal-
482 Wallis ANOVA) to compare coupling differences between systems. To investigate the contributions
483 of various structural predictors, we applied Kruskal-Wallis ANOVA to test the predictive weights
484 derived by Haufe's inversion transform, identifying optimal predictors across regions. We corrected
485 for multiple comparisons using FDR correction. Additionally, we used a general linear model to
486 explore age-related developmental patterns of SC-FC coupling, while controlling for sex,
487 intracranial volume, and in-scanner head motion. Similarly, the system-specific significance of
488 coupling alteration was calculated based on the 1,000 repetitions of the spin test.

489 We examined the associations of SC-FC coupling and its developmental pattern with evolution
490 expansion[35], myelin content[36], and functional principal gradient[37]. Spearman's correlation

analyses were used to quantify the strength of correlations, with significance corrected for spatial autocorrelation with 1,000 repetitions of the spin test.

Prediction of cognitive function. Based on our predictive evaluation work[11], the Elastic-Net algorithm was applied to predict cognitive performance using nodal SC-FC coupling, which tends to yield robust prediction performance across various dimensions of cognitive tasks. The objective function is as follows:

$$L\big(\mathbf{Y}, f(\mathbf{X}, \mathbf{w})\big) = \sum_{i=0}^{n} (y_i - f(\boldsymbol{x}_i))^2 + \alpha \sum_{j=1}^{m} (\beta |w_j| + \frac{1}{2}(1-\beta) \left|\left|w_j\right|\right|^2) \tag{3}$$

where $\mathbf{x} = \{\boldsymbol{x}_1, \boldsymbol{x}_2, \dots, \boldsymbol{x}_n\}$ represents an observation set (e.g., SC-FC coupling) with a sample size of n, and $\mathbf{y} = \{y_1, y_2, \dots, y_n\}$ is a label set (e.g., cognitive measure). The model solves the fitting coefficient $\mathbf{w} = (w_1, w_2, \dots, w_m)$ under the minimization objective function $L\big(\mathbf{Y}, f(\mathbf{X}, \mathbf{w})\big)$. The L1 regular term $|\cdot|$ and L2 regular term $\left|\left|\cdot\right|\right|^2$ constraint the fitting coefficient to ensure model generalization ability. α represents regularization strength, controlling the compression loss scale, and β denotes a trade-off parameter between the L1 and L2 terms.

We employed a nested fivefold cross validation (CV) framework comprising an external CV and an internal CV[11]. In the external CV, observations were randomly partitioned into five folds, with four of them included in the training set used to develop the model and the remaining fold used as a testing set to assess the predictive accuracy of the model. This process was repeated 100 times, and the final model performance was evaluated by averaging the predictive accuracy across the 100 models. In the internal CV, the hyperparameter spaces were first defined as $\alpha \in \{x | x = 2^n, n \in \mathbf{Z}, n \in [-10,5]\}$ and $\beta \in \{x | x = 0.1n, n \in \mathbf{Z}, n \in [0,10]\}$. Then, the training set was further divided into five folds. Four folds composed the internal training set, which was used to generate models by successively applying 16×11 hyperparametric combinations, and the remaining fold was defined as the validation set and used to find the optimal combination. Subsequently, we retrained the model on the training set using the optimal hyperparametric combination and assessed its predictive performance on the testing set by performing Pearson's correlation analyses of the relationship between the predicted and labelled values.

Prior to applying the nested fivefold cross-validation framework to each behaviour measure, we regressed out covariates including sex, intracranial volume, and in-scanner head motion from

the behaviour measure[59, 69]. Specifically, we estimated the regression coefficients of the covariates using the training set and applied them to the testing set. This regression procedure was repeated for each fold. Additionally, we conducted control analyses using age-adjusted behavioral measures to investigate the effect of age on the predictive performance of SC-FC coupling.

To evaluate whether our model performed better than at chance on each behaviour measure, we performed 1,000 permutation tests by randomly shuffling the behaviour measure across participants, generating a null model of predicted performance using the same procedures. We then used the corrected resampled *t* test to determine statistical significance[87, 88]. We corrected for multiple comparisons using FDR correction. For model interpretability, we applied Haufe's inversion transform[38] to obtain predicted weights for various brain regions. The significance of the weights for each system was assessed by comparing them to those generated by a spin test[86] with 1,000 repetitions.

Association between alterations of SC-FC coupling and gene expression. We preprocessed the anatomic and genomic information of the Allen Human Brain Atlas (AHBA) dataset following a recommended pipeline[40]. Specifically, we used FreeSurfer (https://surfer.nmr.mgh.harvard.edu/fswiki/) to generate preprocessed structural data for each donor and projected the BNA template onto native fsaverage space using official scripts (http://www.brainnetome.org/resource/). Finally, we produced an averaged gene expression profile for 10,027 genes covering 105 left cortical regions.

PLS analysis[39] was performed to mine the linear association between the spatial development pattern of SC-FC coupling and gene expression profiles. We used absolute values of the correlation between age and SC-FC coupling in 105 left cortical regions as predicted variables and the gene expression profiles of the corresponding regions as predictor variables. Pearson's correlation coefficient was calculated to determine the association between the PLS score and the absolute correlation value between age and SC-FC coupling. To correct for spatial autocorrelation, we compared the empirically observed value to spatially constrained null models generated by 10,000 spin permutations[86]. We then transformed the gene weight on PLS1 into a z score by dividing the standard deviation of the corresponding weights estimated from bootstrapping, and ranked all genes accordingly. We identified significant genes at a threshold of $p < 0.05$ and classified

them as having positive or negative gene weights. To understand the functional significance of these genes, we performed gene functional enrichment analysis (GO analysis of biological processes and pathways) using Metascape[42]. We focused on the selected genes with positive or negative weights and retained enrichment pathways with an FDR-corrected < 0.05.

To investigate the cell type-specific expression of the selected genes, we assigned them to 58 cell types derived from five studies[43-47] focusing on single-cell research using the human postnatal cortex. To avoid potential bias in cell-type assignment, we grouped these cell types into seven canonical classes: astrocytes, endothelial cells, excitatory neurons, inhibitory neurons, microglia, oligodendrocytes, and OPCs[48, 89]. We generated a null model by performing 10,000 random resamplings of genes within each cell type. We then tested the significance of our results against this null model. Additionally, we subjected the genes associated with each enriched term to the same analysis to explore the specificity of the cell type.

Reproducibility analyses. To evaluate the robustness of our findings under different parcellation templates, using the multimodal parcellation from the Human Connectome Project (HCPMMP)[49], we repeated the network computation of MPC, SCs (WMC, communicability[32], mean first passage times of random walkers[33], and flow graphs (timescales=1)) and FC following the same procedures. Then, we used the multilinear model to examine the association of individual nodewise SC profiles and FC profiles. Finally, a general linear model was used to explore age-related developmental patterns of SC-FC coupling, while controlling for sex, intracranial volume, and in-scanner head motion. We corrected for multiple comparisons using FDR correlation.

To evaluate the sensitivity of our results to deterministic tractography, we used the Camino toolbox (http://camino.cs.ucl.ac.uk/) to reconstruct fibres with a ball-and-stick model estimated from bedpostx results[79] and to generate a fibre number-weighted network using the BNA atlas. We then calculated the communication properties of the WMC using measures such as communicability, mean first passage times of random walkers, and flow graphs (timescales=1). The same pipeline was used for subsequent SC-FC coupling, prediction, and gene analysis. To assess the consistency of our results between deterministic tractography and probabilistic tractography, we performed Pearson's correlation analyses with significance corrected for spatial autocorrelation through 1,000 repetitions of the spin test.

To evaluate the generalizability of our findings, we adopted a split-half cross-validation strategy by randomly partitioning the whole dataset (WD) into two independent subsets (S1 and S2). This process was repeated 1,000 times to minimize bias due to data partitioning. We then used the same procedures to quantify SC-FC coupling, the correlation between age and SC-FC coupling and gene weights in both S1 and S2. Finally, we assessed the consistency of results by calculating Pearson's correlation coefficients of the relationships between S1 and WD, S2 and WD, and S1 and S2.

Data and code availability

The HCP-D 2.0 release data that support the findings of this study are publicly available at https://www.humanconnectome.org/study/hcp-lifespan-development.

Code availability

R4.1.2 software (https://www.r-project.org/) was used to construct the general linear model. MATLAB scripts used for preprocessing of the AHBA dataset can be found at https://github.com/BMHLab/AHBAprocessing. Python scripts used to perform PLS regression can be found at https://scikit-learn.org/. The minimal preprocessing pipelines can be accessed at https://github.com/Washington-University/HCPpipelines. The code relevant to this study can be accessed through the following GitHub repository: https://github.com/FelixFengCN/SC-FC-coupling-development.

Credit Authorship Contribution Statement

G.F. performed acquisition and analysis of data, contributed new analytic tools, drafted and revised the paper. Y.W., W.H., H.C. and J.C. performed acquisition and analysis of data. N.S. contributed to the design of the work, performed analysis of data, and revised the paper.

Acknowledgements

The authors thank all the volunteers for their participation in the study and anonymous reviewers for their insightful comments and suggestions. This work was supported by the STI2030-Major Projects (2021ZD0200500, 2022ZD0213300), National Natural Science Foundation of China (32271145, 81871425), Fundamental Research Funds for the Central Universities (2017XTCX04), Open Research Fund of the State Key Laboratory of Cognitive Neuroscience and Learning (CNLZD2101). Data in this publication were provide (in part) by the Human Connectome Project-Development (HCP-D), which is supported by the National Institute Of Mental Health of the National Institutes of Health under Award Number U01MH109589 and by funds provided by the McDonnell Center for Systems Neuroscience at Washington University in St. Louis.

Financial Disclosures

There are no conflicts of interest including any financial, personal, or other relationships with people or organizations for any of the authors related to the work described in the article.

References

1. Vazquez-Rodriguez B, Suarez LE, Markello RD, Shafiei G, Paquola C, Hagmann P, et al. Gradients of structure-function tethering across neocortex. Proc Natl Acad Sci U S A. 2019;116(42):21219-27. Epub 2019/10/02. doi: 10.1073/pnas.1903403116. PubMed PMID: 31570622; PubMed Central PMCID: PMCPMC6800358.
2. Sarwar T, Tian Y, Yeo BTT, Ramamohanarao K, Zalesky A. Structure-function coupling in the human connectome: A machine learning approach. Neuroimage. 2020;226:117609. Epub 2020/12/04. doi: 10.1016/j.neuroimage.2020.117609. PubMed PMID: 33271268.
3. Demirtas M, Burt JB, Helmer M, Ji JL, Adkinson BD, Glasser MF, et al. Hierarchical Heterogeneity across Human Cortex Shapes Large-Scale Neural Dynamics. Neuron. 2019;101(6):1181-94 e13. Epub 2019/02/13. doi: 10.1016/j.neuron.2019.01.017. PubMed PMID: 30744986; PubMed Central PMCID: PMCPMC6447428.
4. Deco G, Jirsa VK, McIntosh AR. Emerging concepts for the dynamical organization of resting-state activity in the brain. Nat Rev Neurosci. 2011;12(1):43-56. Epub 2010/12/21. doi: 10.1038/nrn2961. PubMed PMID: 21170073.
5. Breakspear M. Dynamic models of large-scale brain activity. Nat Neurosci. 2017;20(3):340-52. Epub 2017/02/24. doi: 10.1038/nn.4497. PubMed PMID: 28230845.
6. Valk SL, Xu T, Paquola C, Park BY, Bethlehem RAI, Vos de Wael R, et al. Genetic and phylogenetic uncoupling of structure and function in human transmodal cortex. Nat Commun. 2022;13(1):2341. Epub 2022/05/10. doi: 10.1038/s41467-022-29886-1. PubMed PMID: 35534454; PubMed Central PMCID: PMCPMC9085871.
7. Zamani Esfahlani F, Faskowitz J, Slack J, Misic B, Betzel RF. Local structure-function relationships in human brain networks across the lifespan. Nat Commun. 2022;13(1):2053. Epub 2022/04/21. doi: 10.1038/s41467-022-29770-y. PubMed PMID: 35440659; PubMed Central PMCID: PMCPMC9018911.
8. Gu Z, Jamison KW, Sabuncu MR, Kuceyeski A. Heritability and interindividual variability of regional structure-function coupling. Nat Commun. 2021;12(1):4894. Epub 2021/08/14. doi: 10.1038/s41467-021-25184-4. PubMed PMID: 34385454; PubMed Central PMCID: PMCPMC8361191.
9. Baum GL, Cui Z, Roalf DR, Ciric R, Betzel RF, Larsen B, et al. Development of structure-function coupling in human brain networks during youth. Proc Natl Acad Sci U S A. 2020;117(1):771-8. Epub 2019/12/26. doi: 10.1073/pnas.1912034117. PubMed PMID: 31874926; PubMed Central PMCID: PMCPMC6955327.
10. Bassett DS, Sporns O. Network neuroscience. Nat Neurosci. 2017;20(3):353-64. Epub 2017/02/24. doi: 10.1038/nn.4502. PubMed PMID: 28230844; PubMed Central PMCID: PMCPMC5485642.
11. Feng G, Wang Y, Huang W, Chen H, Dai Z, Ma G, et al. Methodological evaluation of individual cognitive prediction based on the brain white matter structural connectome. Hum Brain Mapp. 2022;43(12):3775-91. Epub 2022/04/28. doi: 10.1002/hbm.25883. PubMed PMID: 35475571; PubMed Central PMCID: PMCPMC9294303.
12. Paquola C, Vos De Wael R, Wagstyl K, Bethlehem RAI, Hong SJ, Seidlitz J, et al. Microstructural and functional gradients are increasingly dissociated in transmodal cortices. PLoS Biol. 2019;17(5):e3000284. Epub 2019/05/21. doi: 10.1371/journal.pbio.3000284. PubMed PMID:

31107870; PubMed Central PMCID: PMCPMC6544318 following competing interests: Dr. Bullmore is employed half-time by the University of Cambridge and half-time by GlaxoSmithKline (GSK); he holds stock in GSK. The views expressed are those of the authors and not necessarily those of the NHS, the NIHR, GSK or the Department of Health.

13. Liu ZQ, Vazquez-Rodriguez B, Spreng RN, Bernhardt BC, Betzel RF, Misic B. Time-resolved structure-function coupling in brain networks. Commun Biol. 2022;5(1):532. Epub 2022/06/03. doi: 10.1038/s42003-022-03466-x. PubMed PMID: 35654886; PubMed Central PMCID: PMCPMC9163085.

14. Paquola C, Hong SJ. The Potential of Myelin-Sensitive Imaging: Redefining Spatiotemporal Patterns of Myeloarchitecture. Biol Psychiatry. 2023;93(5):442-54. Epub 2022/12/09. doi: 10.1016/j.biopsych.2022.08.031. PubMed PMID: 36481065.

15. Park BY, Paquola C, Bethlehem RAI, Benkarim O, Neuroscience in Psychiatry Network C, Misic B, et al. Adolescent development of multiscale structural wiring and functional interactions in the human connectome. Proc Natl Acad Sci U S A. 2022;119(27):e2116673119. Epub 2022/07/02. doi: 10.1073/pnas.2116673119. PubMed PMID: 35776541; PubMed Central PMCID: PMCPMC9271154.

16. Honey CJ, Sporns O, Cammoun L, Gigandet X, Thiran JP, Meuli R, et al. Predicting human resting-state functional connectivity from structural connectivity. Proc Natl Acad Sci U S A. 2009;106(6):2035-40. Epub 2009/02/04. doi: 10.1073/pnas.0811168106. PubMed PMID: 19188601; PubMed Central PMCID: PMCPMC2634800.

17. Sanz-Leon P, Knock SA, Spiegler A, Jirsa VK. Mathematical framework for large-scale brain network modeling in The Virtual Brain. Neuroimage. 2015;111:385-430. Epub 2015/01/17. doi: 10.1016/j.neuroimage.2015.01.002. PubMed PMID: 25592995.

18. Avena-Koenigsberger A, Misic B, Sporns O. Communication dynamics in complex brain networks. Nat Rev Neurosci. 2017;19(1):17-33. Epub 2017/12/15. doi: 10.1038/nrn.2017.149. PubMed PMID: 29238085.

19. Buckner RL, Krienen FM. The evolution of distributed association networks in the human brain. Trends Cogn Sci. 2013;17(12):648-65. Epub 2013/11/12. doi: 10.1016/j.tics.2013.09.017. PubMed PMID: 24210963.

20. Preti MG, Van De Ville D. Decoupling of brain function from structure reveals regional behavioral specialization in humans. Nat Commun. 2019;10(1):4747. Epub 2019/10/20. doi: 10.1038/s41467-019-12765-7. PubMed PMID: 31628329; PubMed Central PMCID: PMCPMC6800438.

21. Chan SY, Ong ZY, Ngoh ZM, Chong YS, Zhou JH, Fortier MV, et al. Structure-function coupling within the reward network in preschool children predicts executive functioning in later childhood. Developmental cognitive neuroscience. 2022;55:101107. Epub 2022/04/13. doi: 10.1016/j.dcn.2022.101107. PubMed PMID: 35413663; PubMed Central PMCID: PMCPMC9010704.

22. Medaglia JD, Huang W, Karuza EA, Kelkar A, Thompson-Schill SL, Ribeiro A, et al. Functional Alignment with Anatomical Networks is Associated with Cognitive Flexibility. Nat Hum Behav. 2018;2(2):156-64. Epub 2018/12/01. doi: 10.1038/s41562-017-0260-9. PubMed PMID: 30498789; PubMed Central PMCID: PMCPMC6258039.

23. Kuceyeski AF, Jamison KW, Owen JP, Raj A, Mukherjee P. Longitudinal increases in structural connectome segregation and functional connectome integration are associated with better recovery after mild TBI. Hum Brain Mapp. 2019;40(15):4441-56. Epub 2019/07/12. doi: 10.1002/hbm.24713. PubMed PMID: 31294921; PubMed Central PMCID: PMCPMC6865536.

24. Hawrylycz MJ, Lein ES, Guillozet-Bongaarts AL, Shen EH, Ng L, Miller JA, et al. An anatomically comprehensive atlas of the adult human brain transcriptome. Nature. 2012;489(7416):391-9. Epub 2012/09/22. doi: 10.1038/nature11405. PubMed PMID: 22996553; PubMed Central PMCID: PMCPMC4243026.
25. Whitaker KJ, Vertes PE, Romero-Garcia R, Vasa F, Moutoussis M, Prabhu G, et al. Adolescence is associated with genomically patterned consolidation of the hubs of the human brain connectome. Proc Natl Acad Sci U S A. 2016;113(32):9105-10. Epub 2016/07/28. doi: 10.1073/pnas.1601745113. PubMed PMID: 27457931; PubMed Central PMCID: PMCPMC4987797.
26. Arnatkeviciute A, Fulcher BD, Oldham S, Tiego J, Paquola C, Gerring Z, et al. Genetic influences on hub connectivity of the human connectome. Nat Commun. 2021;12(1):4237. Epub 2021/07/11. doi: 10.1038/s41467-021-24306-2. PubMed PMID: 34244483; PubMed Central PMCID: PMCPMC8271018.
27. Fornito A, Arnatkeviciute A, Fulcher BD. Bridging the Gap between Connectome and Transcriptome. Trends Cogn Sci. 2019;23(1):34-50. Epub 2018/11/21. doi: 10.1016/j.tics.2018.10.005. PubMed PMID: 30455082.
28. Paquola C, Bethlehem RA, Seidlitz J, Wagstyl K, Romero-Garcia R, Whitaker KJ, et al. Shifts in myeloarchitecture characterise adolescent development of cortical gradients. Elife. 2019;8. Epub 2019/11/15. doi: 10.7554/eLife.50482. PubMed PMID: 31724948; PubMed Central PMCID: PMCPMC6855802.
29. Xia Y, Xia M, Liu J, Liao X, Lei T, Liang X, et al. Development of functional connectome gradients during childhood and adolescence. Science Bulletin. 2022;67(10):1049-61. doi: 10.1016/j.scib.2022.01.002.
30. Somerville LH, Bookheimer SY, Buckner RL, Burgess GC, Curtiss SW, Dapretto M, et al. The Lifespan Human Connectome Project in Development: A large-scale study of brain connectivity development in 5-21 year olds. Neuroimage. 2018;183:456-68. Epub 2018/08/25. doi: 10.1016/j.neuroimage.2018.08.050. PubMed PMID: 30142446; PubMed Central PMCID: PMCPMC6416053.
31. Fan L, Li H, Zhuo J, Zhang Y, Wang J, Chen L, et al. The Human Brainnetome Atlas: A New Brain Atlas Based on Connectional Architecture. Cereb Cortex. 2016;26(8):3508-26. Epub 2016/05/28. doi: 10.1093/cercor/bhw157. PubMed PMID: 27230218; PubMed Central PMCID: PMCPMC4961028.
32. Crofts JJ, Higham DJ. A weighted communicability measure applied to complex brain networks. Journal of the Royal Society, Interface. 2009;6(33):411-4. Epub 2009/01/15. doi: 10.1098/rsif.2008.0484. PubMed PMID: 19141429; PubMed Central PMCID: PMCPMC2658663.
33. Noh JD, Rieger H. Random walks on complex networks. Physical review letters. 2004;92(11):118701. Epub 2004/04/20. doi: 10.1103/PhysRevLett.92.118701. PubMed PMID: 15089179.
34. Yeo BT, Krienen FM, Sepulcre J, Sabuncu MR, Lashkari D, Hollinshead M, et al. The organization of the human cerebral cortex estimated by intrinsic functional connectivity. J Neurophysiol. 2011;106(3):1125-65. Epub 2011/06/10. doi: 10.1152/jn.00338.2011. PubMed PMID: 21653723; PubMed Central PMCID: PMCPMC3174820.
35. Hill J, Inder T, Neil J, Dierker D, Harwell J, Van Essen D. Similar patterns of cortical expansion during human development and evolution. Proc Natl Acad Sci U S A. 2010;107(29):13135-40. Epub 2010/07/14. doi: 10.1073/pnas.1001229107. PubMed PMID: 20624964; PubMed Central PMCID:

PMCPMC2919958.
36. Glasser MF, Van Essen DC. Mapping human cortical areas in vivo based on myelin content as revealed by T1- and T2-weighted MRI. J Neurosci. 2011;31(32):11597-616. Epub 2011/08/13. doi: 10.1523/JNEUROSCI.2180-11.2011. PubMed PMID: 21832190; PubMed Central PMCID: PMCPMC3167149.
37. Margulies DS, Ghosh SS, Goulas A, Falkiewicz M, Huntenburg JM, Langs G, et al. Situating the default-mode network along a principal gradient of macroscale cortical organization. Proc Natl Acad Sci U S A. 2016;113(44):12574-9. Epub 2016/11/03. doi: 10.1073/pnas.1608282113. PubMed PMID: 27791099; PubMed Central PMCID: PMCPMC5098630.
38. Haufe S, Meinecke F, Gorgen K, Dahne S, Haynes JD, Blankertz B, et al. On the interpretation of weight vectors of linear models in multivariate neuroimaging. Neuroimage. 2014;87:96-110. Epub 2013/11/19. doi: 10.1016/j.neuroimage.2013.10.067. PubMed PMID: 24239590.
39. Krishnan A, Williams LJ, McIntosh AR, Abdi H. Partial Least Squares (PLS) methods for neuroimaging: a tutorial and review. Neuroimage. 2011;56(2):455-75. Epub 2010/07/27. doi: 10.1016/j.neuroimage.2010.07.034. PubMed PMID: 20656037.
40. Arnatkeviciute A, Fulcher BD, Fornito A. A practical guide to linking brain-wide gene expression and neuroimaging data. Neuroimage. 2019;189:353-67. Epub 2019/01/17. doi: 10.1016/j.neuroimage.2019.01.011. PubMed PMID: 30648605.
41. Vos de Wael R, Benkarim O, Paquola C, Lariviere S, Royer J, Tavakol S, et al. BrainSpace: a toolbox for the analysis of macroscale gradients in neuroimaging and connectomics datasets. Commun Biol. 2020;3(1):103. Epub 2020/03/07. doi: 10.1038/s42003-020-0794-7. PubMed PMID: 32139786; PubMed Central PMCID: PMCPMC7058611.
42. Zhou Y, Zhou B, Pache L, Chang M, Khodabakhshi AH, Tanaseichuk O, et al. Metascape provides a biologist-oriented resource for the analysis of systems-level datasets. Nat Commun. 2019;10(1):1523. Epub 2019/04/05. doi: 10.1038/s41467-019-09234-6. PubMed PMID: 30944313; PubMed Central PMCID: PMCPMC6447622.
43. Zhang Y, Sloan SA, Clarke LE, Caneda C, Plaza CA, Blumenthal PD, et al. Purification and Characterization of Progenitor and Mature Human Astrocytes Reveals Transcriptional and Functional Differences with Mouse. Neuron. 2016;89(1):37-53. Epub 2015/12/22. doi: 10.1016/j.neuron.2015.11.013. PubMed PMID: 26687838; PubMed Central PMCID: PMCPMC4707064.
44. Lake BB, Chen S, Sos BC, Fan J, Kaeser GE, Yung YC, et al. Integrative single-cell analysis of transcriptional and epigenetic states in the human adult brain. Nature biotechnology. 2018;36(1):70-80. Epub 2017/12/12. doi: 10.1038/nbt.4038. PubMed PMID: 29227469; PubMed Central PMCID: PMCPMC5951394.
45. Habib N, Avraham-Davidi I, Basu A, Burks T, Shekhar K, Hofree M, et al. Massively parallel single-nucleus RNA-seq with DroNc-seq. Nat Methods. 2017;14(10):955-8. Epub 2017/08/29. doi: 10.1038/nmeth.4407. PubMed PMID: 28846088; PubMed Central PMCID: PMCPMC5623139.
46. Darmanis S, Sloan SA, Zhang Y, Enge M, Caneda C, Shuer LM, et al. A survey of human brain transcriptome diversity at the single cell level. Proc Natl Acad Sci U S A. 2015;112(23):7285-90. Epub 2015/06/11. doi: 10.1073/pnas.1507125112. PubMed PMID: 26060301; PubMed Central PMCID: PMCPMC4466750.
47. Li M, Santpere G, Imamura Kawasawa Y, Evgrafov OV, Gulden FO, Pochareddy S, et al. Integrative functional genomic analysis of human brain development and neuropsychiatric risks.

Science. 2018;362(6420). Epub 2018/12/14. doi: 10.1126/science.aat7615. PubMed PMID: 30545854; PubMed Central PMCID: PMCPMC6413317.
48. Seidlitz J, Nadig A, Liu S, Bethlehem RAI, Vértes PE, Morgan SE, et al. Transcriptomic and cellular decoding of regional brain vulnerability to neurogenetic disorders. Nat Commun. 2020;11(1):3358. Epub 2020/07/06. doi: 10.1038/s41467-020-17051-5. PubMed PMID: 32620757; PubMed Central PMCID: PMCPMC7335069.
49. Glasser MF, Coalson TS, Robinson EC, Hacker CD, Harwell J, Yacoub E, et al. A multi-modal parcellation of human cerebral cortex. Nature. 2016;536(7615):171-8. Epub 2016/07/21. doi: 10.1038/nature18933. PubMed PMID: 27437579; PubMed Central PMCID: PMCPMC4990127.
50. Damoiseaux JS, Greicius MD. Greater than the sum of its parts: a review of studies combining structural connectivity and resting-state functional connectivity. Brain Struct Funct. 2009;213(6):525-33. Epub 2009/07/01. doi: 10.1007/s00429-009-0208-6. PubMed PMID: 19565262.
51. Wang P, Kong R, Kong X, Liégeois R, Orban C, Deco G, et al. Inversion of a large-scale circuit model reveals a cortical hierarchy in the dynamic resting human brain. Sci Adv. 2019;5(1):eaat7854. Epub 2019/01/22. doi: 10.1126/sciadv.aat7854. PubMed PMID: 30662942; PubMed Central PMCID: PMCPMC6326747.
52. Woolrich MW, Stephan KE. Biophysical network models and the human connectome. Neuroimage. 2013;80:330-8. Epub 2013/04/11. doi: 10.1016/j.neuroimage.2013.03.059. PubMed PMID: 23571421.
53. Messé A, Rudrauf D, Giron A, Marrelec G. Predicting functional connectivity from structural connectivity via computational models using MRI: an extensive comparison study. Neuroimage. 2015;111:65-75. Epub 2015/02/17. doi: 10.1016/j.neuroimage.2015.02.001. PubMed PMID: 25682944.
54. Honey CJ, Kötter R, Breakspear M, Sporns O. Network structure of cerebral cortex shapes functional connectivity on multiple time scales. Proc Natl Acad Sci U S A. 2007;104(24):10240-5. Epub 2007/06/06. doi: 10.1073/pnas.0701519104. PubMed PMID: 17548818; PubMed Central PMCID: PMCPMC1891224.
55. Goñi J, van den Heuvel MP, Avena-Koenigsberger A, Velez de Mendizabal N, Betzel RF, Griffa A, et al. Resting-brain functional connectivity predicted by analytic measures of network communication. Proc Natl Acad Sci U S A. 2014;111(2):833-8. Epub 2014/01/01. doi: 10.1073/pnas.1315529111. PubMed PMID: 24379387; PubMed Central PMCID: PMCPMC3896172.
56. Avena-Koenigsberger A, Yan X, Kolchinsky A, van den Heuvel MP, Hagmann P, Sporns O. A spectrum of routing strategies for brain networks. PLoS Comput Biol. 2019;15(3):e1006833. Epub 2019/03/09. doi: 10.1371/journal.pcbi.1006833. PubMed PMID: 30849087; PubMed Central PMCID: PMCPMC6426276.
57. Deco G, Kringelbach ML, Arnatkeviciute A, Oldham S, Sabaroedin K, Rogasch NC, et al. Dynamical consequences of regional heterogeneity in the brain's transcriptional landscape. Sci Adv. 2021;7(29). Epub 2021/07/16. doi: 10.1126/sciadv.abf4752. PubMed PMID: 34261652; PubMed Central PMCID: PMCPMC8279501.
58. Huntenburg JM, Bazin PL, Margulies DS. Large-Scale Gradients in Human Cortical Organization. Trends Cogn Sci. 2018;22(1):21-31. Epub 2017/12/06. doi: 10.1016/j.tics.2017.11.002. PubMed PMID: 29203085.
59. Chen J, Tam A, Kebets V, Orban C, Ooi LQR, Asplund CL, et al. Shared and unique brain

network features predict cognitive, personality, and mental health scores in the ABCD study. Nat Commun. 2022;13(1):2217. Epub 2022/04/27. doi: 10.1038/s41467-022-29766-8. PubMed PMID: 35468875; PubMed Central PMCID: PMCPMC9038754.
60. Simons M, Nave KA. Oligodendrocytes: Myelination and Axonal Support. Cold Spring Harbor perspectives in biology. 2015;8(1):a020479. Epub 2015/06/24. doi: 10.1101/cshperspect.a020479. PubMed PMID: 26101081; PubMed Central PMCID: PMCPMC4691794.
61. Berry K, Wang J, Lu QR. Epigenetic regulation of oligodendrocyte myelination in developmental disorders and neurodegenerative diseases. F1000Research. 2020;9. Epub 2020/02/25. doi: 10.12688/f1000research.20904.1. PubMed PMID: 32089836; PubMed Central PMCID: PMCPMC7014579.
62. Gibson EM, Purger D, Mount CW, Goldstein AK, Lin GL, Wood LS, et al. Neuronal activity promotes oligodendrogenesis and adaptive myelination in the mammalian brain. Science. 2014;344(6183):1252304. Epub 2014/04/15. doi: 10.1126/science.1252304. PubMed PMID: 24727982; PubMed Central PMCID: PMCPMC4096908.
63. Mount CW, Monje M. Wrapped to Adapt: Experience-Dependent Myelination. Neuron. 2017;95(4):743-56. Epub 2017/08/18. doi: 10.1016/j.neuron.2017.07.009. PubMed PMID: 28817797; PubMed Central PMCID: PMCPMC5667660.
64. Kurshan PT, Shen K. Synaptogenic pathways. Curr Opin Neurobiol. 2019;57:156-62. Epub 2019/04/16. doi: 10.1016/j.conb.2019.03.005. PubMed PMID: 30986749.
65. Van Horn MR, Ruthazer ES. Glial regulation of synapse maturation and stabilization in the developing nervous system. Curr Opin Neurobiol. 2019;54:113-9. Epub 2018/10/23. doi: 10.1016/j.conb.2018.10.002. PubMed PMID: 30347385.
66. Faust TE, Gunner G, Schafer DP. Mechanisms governing activity-dependent synaptic pruning in the developing mammalian CNS. Nat Rev Neurosci. 2021;22(11):657-73. Epub 2021/09/22. doi: 10.1038/s41583-021-00507-y. PubMed PMID: 34545240; PubMed Central PMCID: PMCPMC8541743.
67. Favuzzi E, Deogracias R, Marques-Smith A, Maeso P, Jezequel J, Exposito-Alonso D, et al. Distinct molecular programs regulate synapse specificity in cortical inhibitory circuits. Science. 2019;363(6425):413-7. Epub 2019/01/27. doi: 10.1126/science.aau8977. PubMed PMID: 30679375.
68. Ciric R, Wolf DH, Power JD, Roalf DR, Baum GL, Ruparel K, et al. Benchmarking of participant-level confound regression strategies for the control of motion artifact in studies of functional connectivity. Neuroimage. 2017;154:174-87. Epub 2017/03/18. doi: 10.1016/j.neuroimage.2017.03.020. PubMed PMID: 28302591; PubMed Central PMCID: PMCPMC5483393.
69. Li J, Bzdok D, Chen J, Tam A, Ooi LQR, Holmes AJ, et al. Cross-ethnicity/race generalization failure of behavioral prediction from resting-state functional connectivity. Sci Adv. 2022;8(11):eabj1812. Epub 2022/03/17. doi: 10.1126/sciadv.abj1812. PubMed PMID: 35294251; PubMed Central PMCID: PMCPMC8926333.
70. Glasser MF, Sotiropoulos SN, Wilson JA, Coalson TS, Fischl B, Andersson JL, et al. The minimal preprocessing pipelines for the Human Connectome Project. Neuroimage. 2013;80:105-24. Epub 2013/05/15. doi: 10.1016/j.neuroimage.2013.04.127. PubMed PMID: 23668970; PubMed Central PMCID: PMCPMC3720813.
71. Thomas C, Ye FQ, Irfanoglu MO, Modi P, Saleem KS, Leopold DA, et al. Anatomical accuracy of brain connections derived from diffusion MRI tractography is inherently limited. Proc Natl Acad

877 Sci U S A. 2014;111(46):16574-9. Epub 2014/11/05. doi: 10.1073/pnas.1405672111. PubMed PMID:
878 25368179; PubMed Central PMCID: PMCPMC4246325.
879 72. Reveley C, Seth AK, Pierpaoli C, Silva AC, Yu D, Saunders RC, et al. Superficial white matter
880 fiber systems impede detection of long-range cortical connections in diffusion MR tractography.
881 Proc Natl Acad Sci U S A. 2015;112(21):E2820-8. Epub 2015/05/13. doi: 10.1073/pnas.1418198112.
882 PubMed PMID: 25964365; PubMed Central PMCID: PMCPMC4450402.
883 73. Kang HJ, Kawasawa YI, Cheng F, Zhu Y, Xu X, Li M, et al. Spatio-temporal transcriptome of
884 the human brain. Nature. 2011;478(7370):483-9. Epub 2011/10/28. doi: 10.1038/nature10523.
885 PubMed PMID: 22031440; PubMed Central PMCID: PMCPMC3566780.
886 74. Harms MP, Somerville LH, Ances BM, Andersson J, Barch DM, Bastiani M, et al. Extending the
887 Human Connectome Project across ages: Imaging protocols for the Lifespan Development and
888 Aging projects. Neuroimage. 2018;183:972-84. Epub 2018/09/28. doi:
889 10.1016/j.neuroimage.2018.09.060. PubMed PMID: 30261308; PubMed Central PMCID:
890 PMCPMC6484842.
891 75. Waehnert MD, Dinse J, Weiss M, Streicher MN, Waehnert P, Geyer S, et al. Anatomically
892 motivated modeling of cortical laminae. Neuroimage. 2014;93 Pt 2:210-20. Epub 2013/04/23. doi:
893 10.1016/j.neuroimage.2013.03.078. PubMed PMID: 23603284.
894 76. Behrens TE, Woolrich MW, Jenkinson M, Johansen-Berg H, Nunes RG, Clare S, et al.
895 Characterization and propagation of uncertainty in diffusion-weighted MR imaging. Magn Reson
896 Med. 2003;50(5):1077-88. Epub 2003/10/31. doi: 10.1002/mrm.10609. PubMed PMID: 14587019.
897 77. Jbabdi S, Sotiropoulos SN, Savio AM, Grana M, Behrens TE. Model-based analysis of
898 multishell diffusion MR data for tractography: how to get over fitting problems. Magn Reson Med.
899 2012;68(6):1846-55. Epub 2012/02/16. doi: 10.1002/mrm.24204. PubMed PMID: 22334356;
900 PubMed Central PMCID: PMCPMC3359399.
901 78. Behrens TE, Berg HJ, Jbabdi S, Rushworth MF, Woolrich MW. Probabilistic diffusion
902 tractography with multiple fibre orientations: What can we gain? Neuroimage. 2007;34(1):144-55.
903 Epub 2006/10/31. doi: 10.1016/j.neuroimage.2006.09.018. PubMed PMID: 17070705; PubMed
904 Central PMCID: PMCPMC7116582.
905 79. Hernandez M, Guerrero GD, Cecilia JM, Garcia JM, Inuggi A, Jbabdi S, et al. Accelerating fibre
906 orientation estimation from diffusion weighted magnetic resonance imaging using GPUs. PLoS
907 One. 2013;8(4):e61892. Epub 2013/05/10. doi: 10.1371/journal.pone.0061892. PubMed PMID:
908 23658616; PubMed Central PMCID: PMCPMC3643787.
909 80. Hernandez-Fernandez M, Reguly I, Jbabdi S, Giles M, Smith S, Sotiropoulos SN. Using GPUs
910 to accelerate computational diffusion MRI: From microstructure estimation to tractography and
911 connectomes. Neuroimage. 2019;188:598-615. Epub 2018/12/12. doi:
912 10.1016/j.neuroimage.2018.12.015. PubMed PMID: 30537563; PubMed Central PMCID:
913 PMCPMC6614035.
914 81. Roberts JA, Perry A, Roberts G, Mitchell PB, Breakspear M. Consistency-based thresholding
915 of the human connectome. Neuroimage. 2017;145(Pt A):118-29. Epub 2016/09/27. doi:
916 10.1016/j.neuroimage.2016.09.053. PubMed PMID: 27666386.
917 82. Rosvall M, Grönlund A, Minnhagen P, Sneppen K. Searchability of networks. Physical review
918 E, Statistical, nonlinear, and soft matter physics. 2005;72(4 Pt 2):046117. Epub 2005/12/31. doi:
919 10.1103/PhysRevE.72.046117. PubMed PMID: 16383478.
920 83. Hilgetag CC, Burns GA, O'Neill MA, Scannell JW, Young MP. Anatomical connectivity defines

the organization of clusters of cortical areas in the macaque monkey and the cat. Philos Trans R Soc Lond B Biol Sci. 2000;355(1393):91-110. Epub 2000/03/07. doi: 10.1098/rstb.2000.0551. PubMed PMID: 10703046; PubMed Central PMCID: PMCPMC1692723.

84. Seguin C, van den Heuvel MP, Zalesky A. Navigation of brain networks. Proc Natl Acad Sci U S A. 2018;115(24):6297-302. Epub 2018/06/01. doi: 10.1073/pnas.1801351115. PubMed PMID: 29848631; PubMed Central PMCID: PMCPMC6004443.

85. Lambiotte R, Sinatra R, Delvenne JC, Evans TS, Barahona M, Latora V. Flow graphs: interweaving dynamics and structure. Physical review E, Statistical, nonlinear, and soft matter physics. 2011;84(1 Pt 2):017102. Epub 2011/08/27. doi: 10.1103/PhysRevE.84.017102. PubMed PMID: 21867345.

86. Alexander-Bloch AF, Shou H, Liu S, Satterthwaite TD, Glahn DC, Shinohara RT, et al. On testing for spatial correspondence between maps of human brain structure and function. Neuroimage. 2018;178:540-51. Epub 2018/06/04. doi: 10.1016/j.neuroimage.2018.05.070. PubMed PMID: 29860082; PubMed Central PMCID: PMCPMC6095687.

87. Bouckaert RR, Frank E. In Advances in Knowledge Discovery and Data Mining 3–12. Springer. 2004.

88. Nadeau C, Bengio Y. Inference for the Generalization Error. Mach Learn. 2003;52:239–81.

89. Li J, Wu GR, Li B, Fan F, Zhao X, Meng Y, et al. Transcriptomic and macroscopic architectures of intersubject functional variability in human brain white-matter. Commun Biol. 2021;4(1):1417. Epub 2021/12/22. doi: 10.1038/s42003-021-02952-y. PubMed PMID: 34931033; PubMed Central PMCID: PMCPMC8688465.

Supplementary Material

Content:

- **Text S1.** The definition of the communication model.
- **Table S1.** Predictive significance of the communication model.
- **Figure S1.** Aged-related changes in MPC weight.
- **Figure S2.** Aged-related changes in communicability weight.
- **Figure S3.** Aged-related changes in flow graphs weight.
- **Figure S4.** Aged-related changes in the weight of the mean first passage time.
- **Figure S5.** Predictive accuracy of regional SC-FC coupling across cognitive measures.
- **Figure S6.** Cell-specific expression in each pathway.
- **Figure S7.** Reproducibility analyses with different parcellation templates (HCPMMP).
- **Figure S8.** Reproducibility analyses with different tractography strategies.
- **Figure S9.** Reproducibility analyses with split-half validation.
- **References**

Supplemental Text

Text S1. The definition of the communication model

Shortest path length

The connectivity of network can be associated with cost, in which higher connectivity strength has lower cost. Let there be a source node s, and a target node t, $p_{s\to t} = \{p_{si}, p_{ij}, \dots, p_{kt}\}$ is the sequence of paths between s and t. Here, a transformation strategy $tp_{si} = p_{ij}^{-\gamma}$ is used to obtain the $tp_{s\to t} = \{tp_{si}, tp_{ij}, \dots, tp_{kt}\}$. The shortest path length $sp_{s\to t}$ is calculated as the minimized sum of $tp_{s\to t}$. We set $\gamma = 0.12, 0.25, 0.5, 1, 2,$ and 4.

Communicability

Communicability[1] is a weighted sum of walks along all connections. The weighted connectivity matrix $\mathbf{A}$ is normalized as $\mathbf{A}' = \mathbf{D}^{-1/2}\mathbf{A}\mathbf{D}^{-1/2}$, where $\mathbf{D}$ is the degree diagonal matrix. The communicability is exponentiated as $\mathbf{G} = e^{\mathbf{A}'}$.

Cosine similarity. Cosine similarity $c_{st} = \frac{\boldsymbol{n}_s \cdot \boldsymbol{n}_t}{\|\boldsymbol{n}_s\| \cdot \|\boldsymbol{n}_t\|}$ measures the angle between connection patterns of two nodes, $\boldsymbol{n}_s = [n_{s1}, n_{s2}, \dots, n_{sm}]$ and $\boldsymbol{n}_t = [n_{t1}, n_{t2}, \dots, n_{tm}]$, where $\|\cdot\|$ is the norm of the vector, and m is the number of brain regions.

Search information

Search information[2] quantifies the amount of information (in bits) required to traverse shortest paths in a network. If the node sequence of shortest path between s and t is given by $|sp_{s\to t}| = \{s, i, j, \dots, k, l, t\}$, then the probability of taking that path is given by $B(sp_{s\to t}) = B_{si} \times B_{ij} \times \dots \times B_{kl} \times B_{lt}$, where $B_{ij} = \frac{p_{ij}}{\sum_j p_{ij}}$. The information transmitted along this path, is then $si(sp_{s\to t}) = \log_2[B(sp_{s\to t})]$.

Matching index

The matching index[3] is a measure of overlap between pairs of nodes based on their connectivity profiles excluding their mutual connections, here defined as $mi_{ij} = \frac{\sum_{i\neq s,t}(p_{si}+p_{it})\theta(p_{si})\theta(p_{it})}{\sum_{i\neq t} p_{si} + \sum_{i\neq s} p_{it}}$, where $\theta(p_{si}) = 1$ if $p_{si} > 0$ and 0 otherwise.

Path transitivity

Path transitivity [4] captures the transitivity of the path linking source nodes to a target node or, put differently, the density of local detours that are available along the path. This leads to the

definition of "path transitivity" as $pt_{st} = \frac{2\sum_{i \in sp_{s\to t}} \sum_{j \in sp_{s\to t}} mi_{ij}}{|sp_{s\to t}|(|sp_{s\to t}|-\mathbf{1})}$.

Greedy navigation.

Greedy navigation[5] is defined as the number of hops in the complete paths revealed by the navigation process. Note that for some node pairs, the navigation procedure leads to a dead end or a cycle- in which case the number of hops is listed as ∞.

Mean first passage times of random walkers

The mean first passage times of random walkers[6] refers to the expected number of steps in a random walk starting at node s to ending at node t.

Flow graphs

Flow graphs[7] are a transformation of a network's (possibly sparse) connectivity matrix $\mathbf{A}$ into a fully-weighted matrix in which the dynamics of a Markov process are embedded into edge weights. For a continuous random walk with dynamics $r_i = -\sum_j L_{ij} r_j$ on node i, the corresponding flow graph is given by $g(t)_{ij} = (e^{-t\mathbf{L}})_{ij} s_j$. In these expressions, the matrix $\mathbf{L} = \mathbf{D} - \mathbf{A}/\mathbf{s}$ is the normalized Laplacian, where $s_i = \sum_j A_{ij}$ is a node's degree or weighted degree and $\mathbf{D}$ is the degree diagonal matrix (a square matrix the elements of s along its diagonal), and $g(t)_{ij}$ represents the probabilistic flow of random walkers between nodes i and j at time t. Here, we generated flow graphs using both binary and weighted structural connectivity matrices and evaluated them at different Markov times, t. Specifically, we focused on t = 1, 2.5, 5, and 10.

Supplemental Tables

Table S1. Predictive significance of the communication model.

Predictor		p_{spin}	Predictor		p_{spin}
Shortest path length	gamma values=0.12	0.93	Path transitivity	weight-to-cost transformations=0.12	0.84
	gamma values=0.25	0.69		weight-to-cost transformations=0.25	0.97
	gamma values=0.5	0.63		weight-to-cost transformations=0.5	0.90
	gamma values=1	0.89		weight-to-cost transformations=1	0.75
	gamma values=2	0.77		weight-to-cost transformations=2	0.90
	gamma values=4	0.45		weight-to-cost transformations=4	0.61
Communicability		<0.001	Matching index		0.42
Cosine similarity		0.25	Greedy navigation		0.99
Search information	weight-to-cost transformations=0.12	0.63	Mean first passage times of random walkers		0.01
	weight-to-cost transformations=0.25	0.59	Flow graphs	timescales=1	<0.001
	weight-to-cost transformations=0.5	0.32		timescales=2.5	0.26
	weight-to-cost transformations=1	0.72		timescales=5	0.91
	weight-to-cost transformations=2	0.60		timescales=10	0.80
	weight-to-cost transformations=4	0.75			

Note: p_{spin}: spin test.

Supplemental Figures

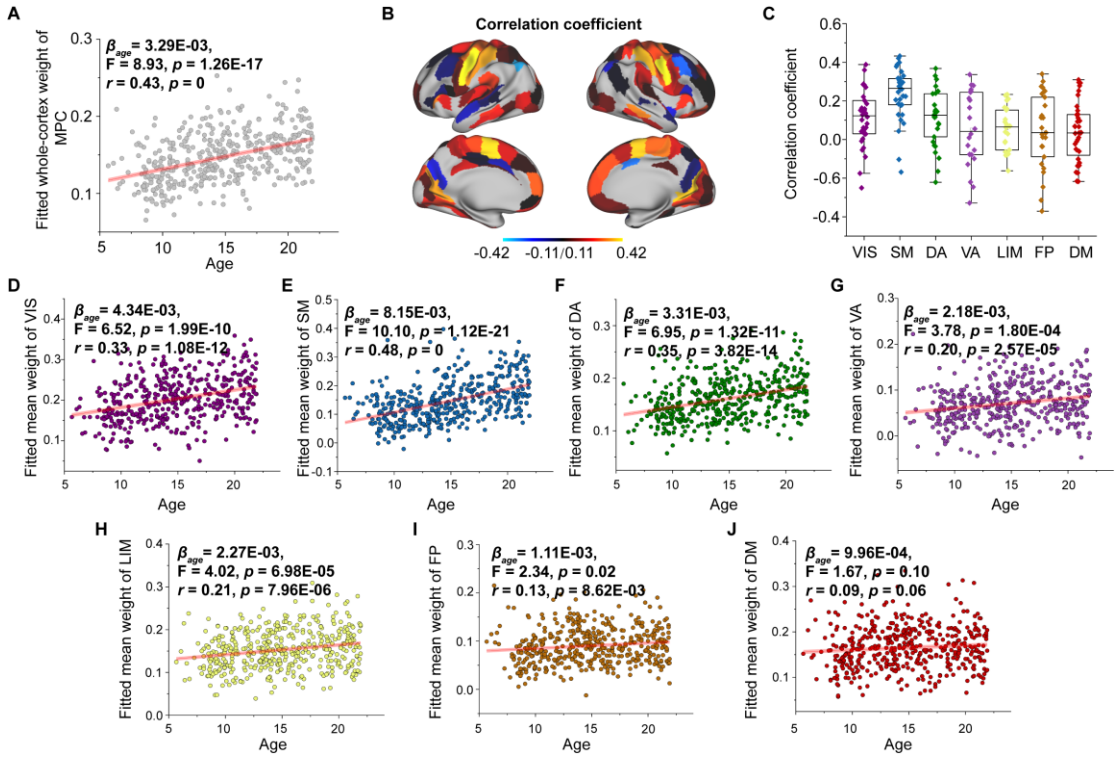

Figure S1. Age-related changes in MPC weight. (A) Increases in MPC weight across the whole-brain with age. (B) Correlation of age with MPC weight across significant regions (p<0.05, FDR corrected). (C) Comparison of changes in MPC weight among functional subnetworks. The boxes show the median and interquartile range (IQR; 25–75%), and the whiskers depict 1.5× IQR from the first or third quartile. (D-J) Correlation of age with MPC weight across the VIS, SM, DA, VA, LIM, FP and DM. VIS, visual network; SM, somatomotor network; DA, dorsal attention network; VA, ventral attention network; LIM, limbic network; FP, frontoparietal network; DM, default mode network.

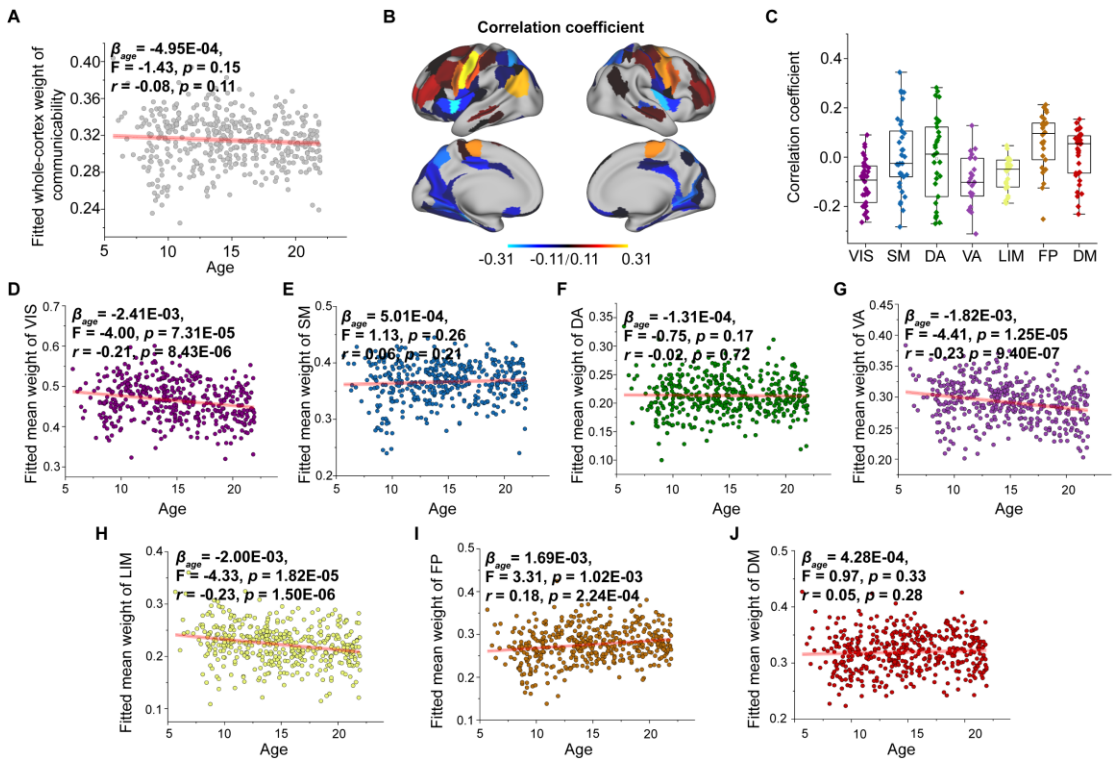

Figure S2. Age-related changes in communicability weight. (A) Increases in communicability weight across the whole brain with age. (B) Correlation of age with communicability weight across significant regions (p<0.05, FDR corrected). (C) Comparison of changes in communicability weight among functional subnetworks. The boxes show the median and interquartile range (IQR; 25–75%), and the whiskers depict 1.5× IQR from the first or third quartile. (D-J) Correlation of age with communicability weight across the VIS, SM, DA, VA, LIM, FP and DM. VIS, visual network; SM, somatomotor network; DA, dorsal attention network; VA, ventral attention network; LIM, limbic network; FP, frontoparietal network; DM, default mode network.

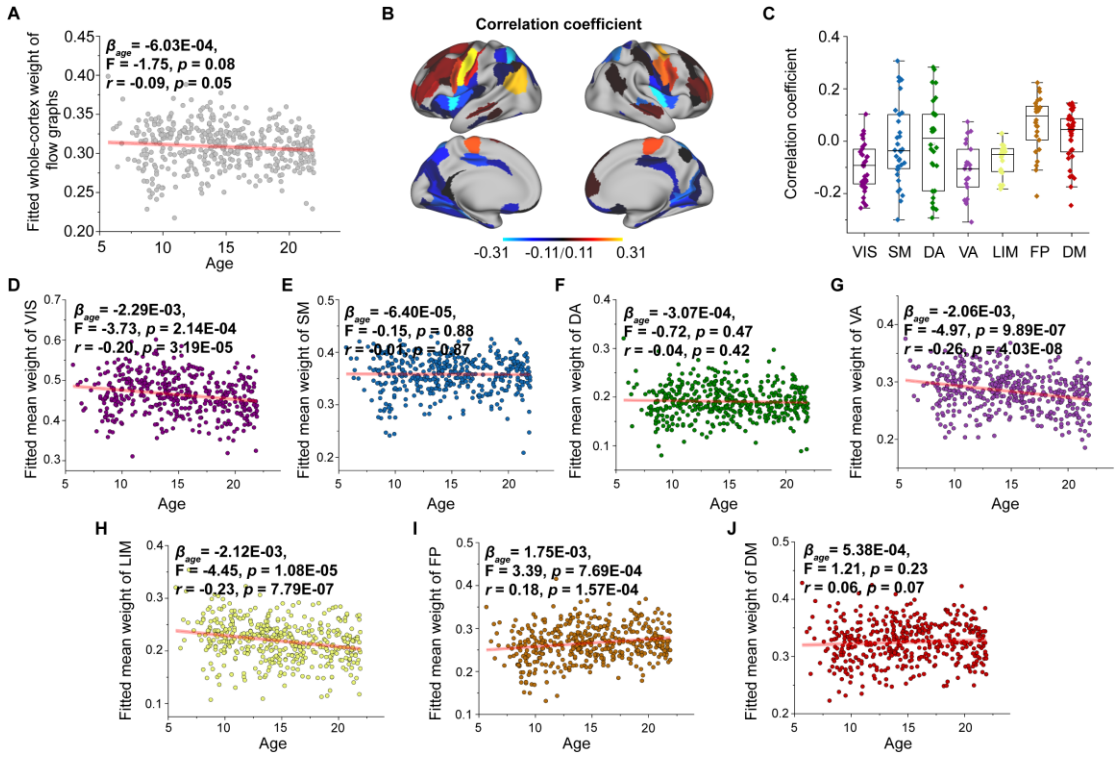

Figure S3. Age-related changes in flow graph weight. (A) Increases in flow graph weight across the whole brain with age. (B) Correlation of age with flow graph weight across significant regions (p<0.05, FDR corrected). (C) Flow graphs of changes in weight among functional networks. The boxes show the median and interquartile range (IQR; 25–75%), and the whiskers depict 1.5× IQR from the first or third quartile. (D-J) Correlation of age with flow graph weight across the VIS, SM, DA, VA, LIM, FP and DM. VIS, visual network; SM, somatomotor network; DA, dorsal attention network; VA, ventral attention network; LIM, limbic network; FP, frontoparietal network; DM, default mode network.

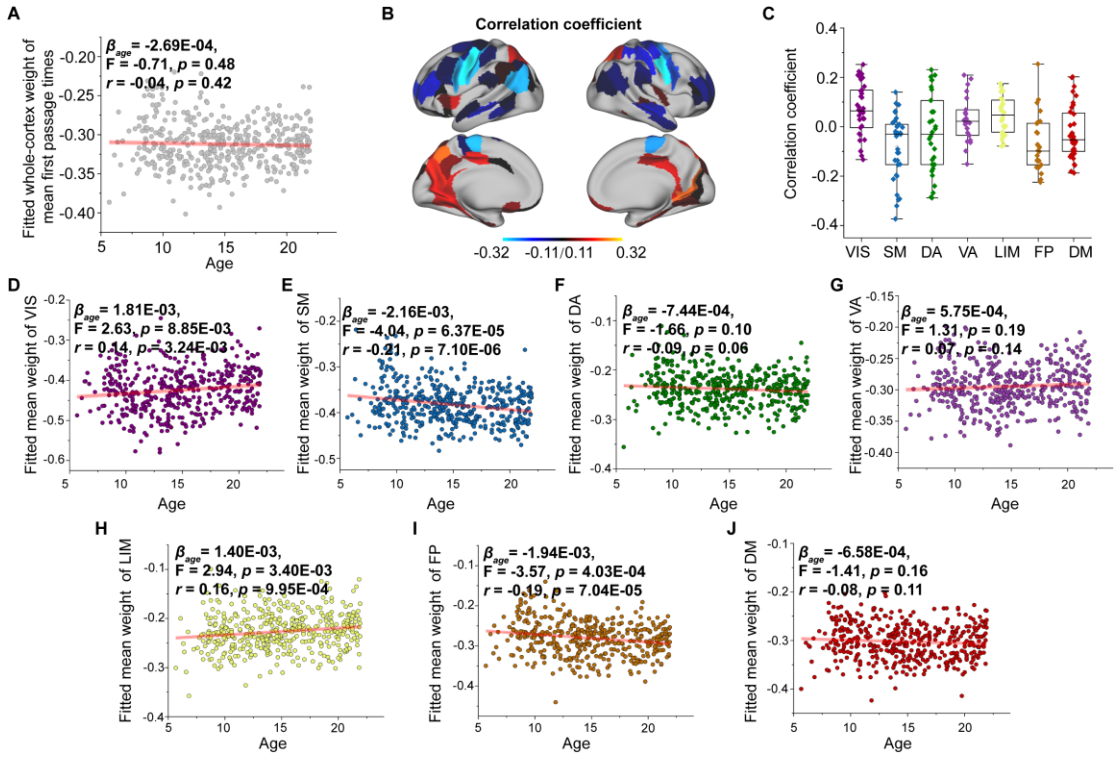

Figure S4. Age-related changes in the weight of the mean first-passage time. (A) Increases in the weight of the mean first-passage time across the whole brain with age. (B) Correlation of age with mean first-passage time weight across significant regions (p<0.05, FDR corrected). (C) Comparison of changes in mean first-passage time weight among functional networks. The boxes show the median and interquartile range (IQR; 25–75%), and the whiskers depict 1.5× IQR from the first or third quartile. (D-J) Correlation of age with mean first-passage time weight across the VIS, SM, DA, VA, LIM, FP and DM. VIS, visual network; SM, somatomotor network; DA, dorsal attention network; VA, ventral attention network; LIM, limbic network; FP, frontoparietal network; DM, default mode network.

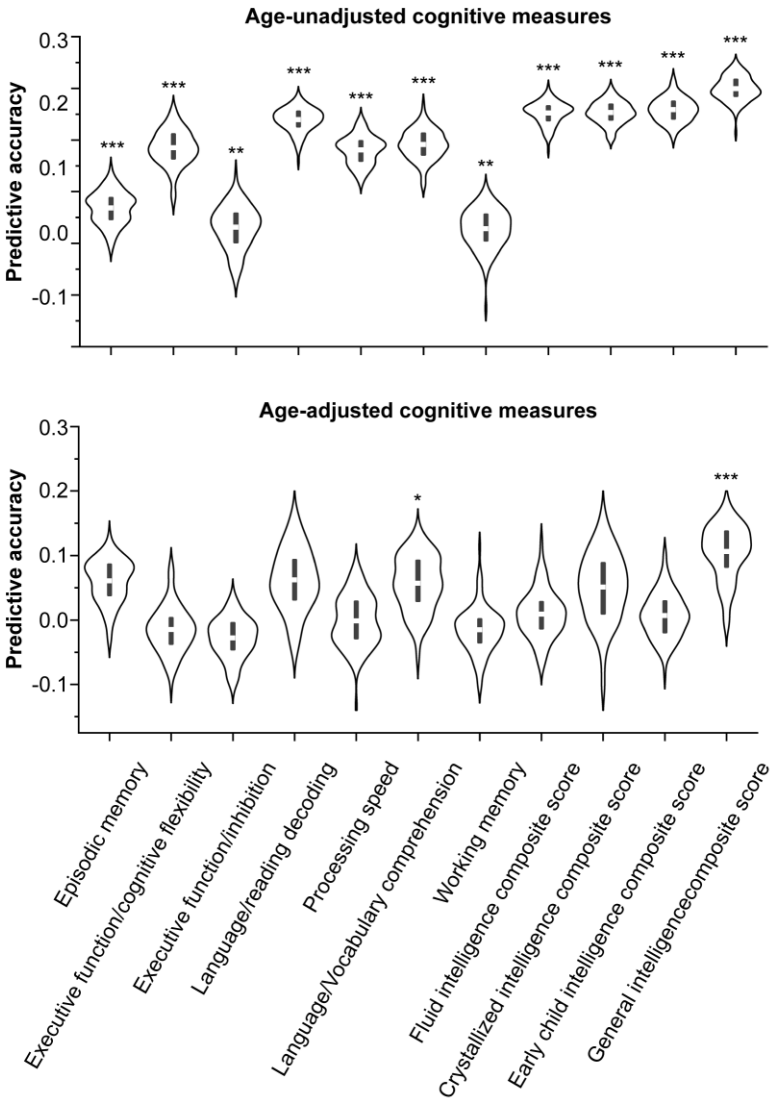

Figure S5. Predictive accuracy of regional SC-FC coupling across cognitive measures. The top panel shows the predictive accuracy of regional SC-FC coupling across cognitive measures not adjusted for age, and the bottom panel shows the predictive accuracy across age-adjusted cognitive measures. Note: ***: $p<0.001$; **: $p<0.01$; *: $p<0.05$; *n.s.*: $p>0.05$.

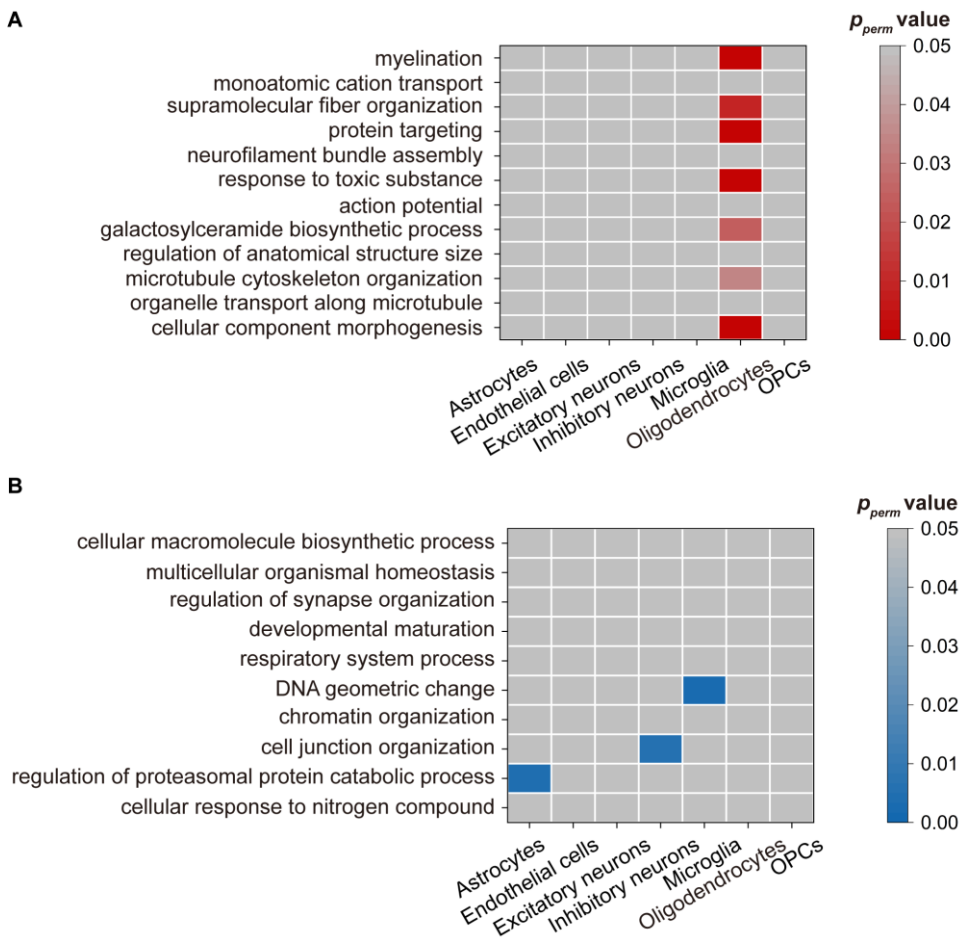

Figure S6. Cell-specific expression in each pathway. (A) Genes with positive weights. (B) Genes with negative weights. Note: p_{perm}: permutation test.

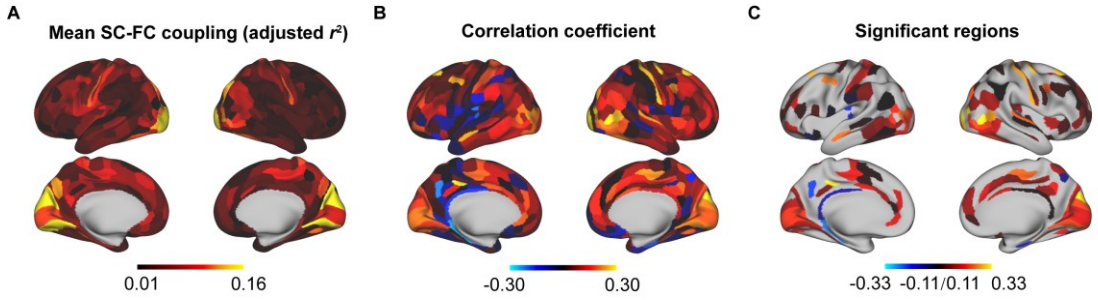

Figure S7. Reproducibility analyses with different parcellation templates (HCPMMP). (A) Spatial pattern of SC-FC coupling. (B) Correlation of age with SC-FC coupling. (C) Correlation of age with SC-FC coupling across significant regions (p<0.05, FDR corrected).

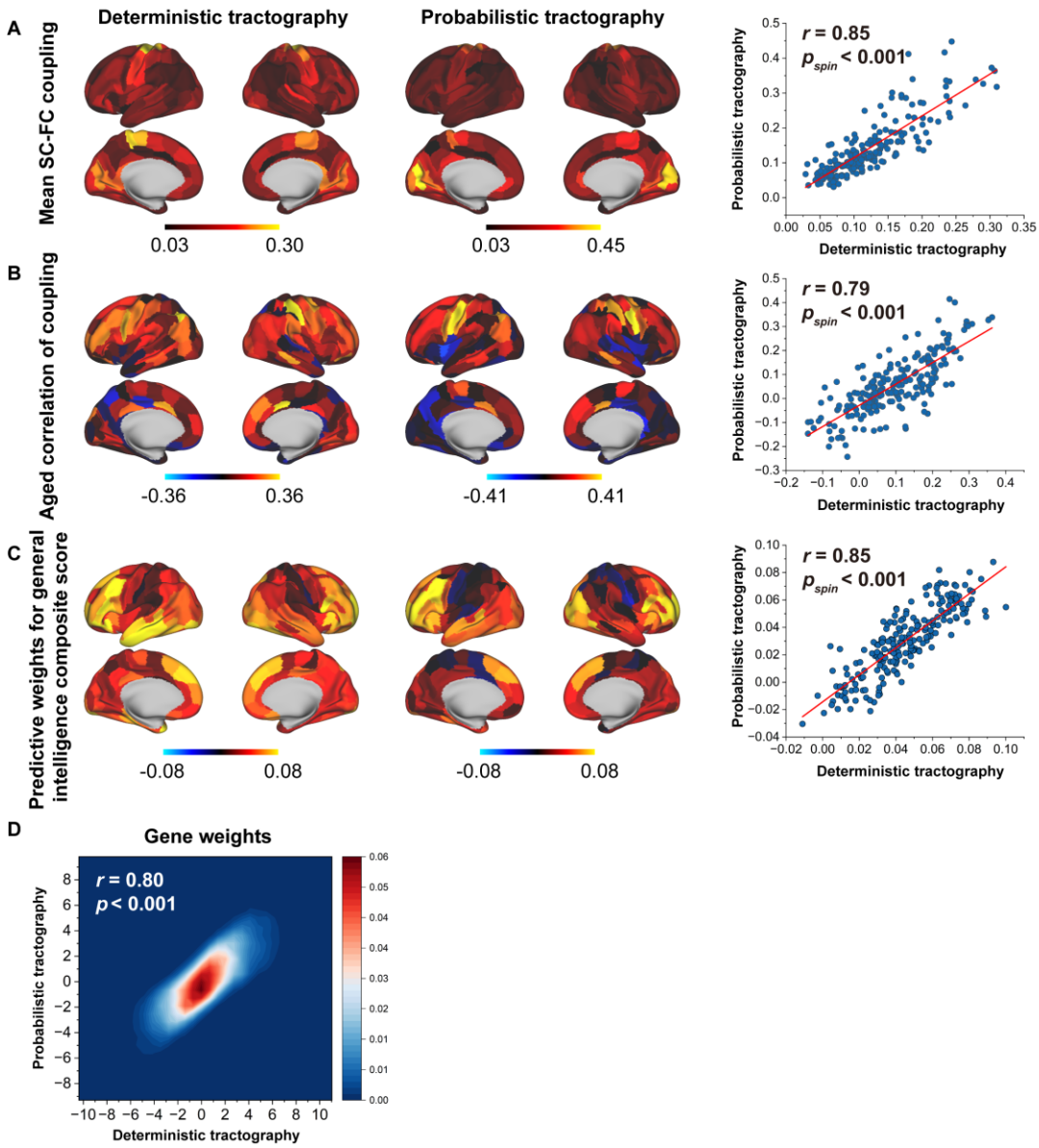

Figure S8. Reproducibility analyses with different tractography strategies. (A) The consistency of mean SC-FC coupling between deterministic tractography and probabilistic tractography. (B) The consistency of the correlation between age and SC-FC coupling between deterministic tractography and probabilistic tractography. (C) The consistent predictive weights for the general intelligence composite score between deterministic tractography and probabilistic tractography. (D) The consistency of gene weights between deterministic tractography and probabilistic tractography.

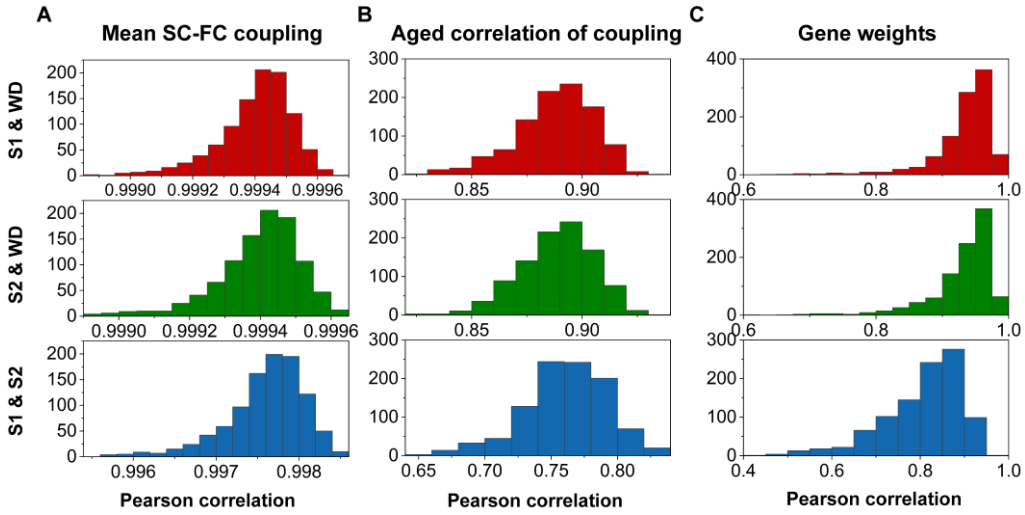

Figure S9. Reproducibility analyses with split-half validation. (A) The consistency of mean SC-FC coupling among S1, S2, and the WD. (B) The consistency of the correlation between age and SC-FC coupling among S1, S2, and the WD. (C) Consistent gene weights among S1, S2, and WD.

References

1. Crofts JJ, Higham DJ. A weighted communicability measure applied to complex brain networks. Journal of the Royal Society, Interface. 2009;6(33):411-4. Epub 2009/01/15. doi: 10.1098/rsif.2008.0484. PubMed PMID: 19141429; PubMed Central PMCID: PMCPMC2658663.
2. Rosvall M, Grönlund A, Minnhagen P, Sneppen K. Searchability of networks. Physical review E, Statistical, nonlinear, and soft matter physics. 2005;72(4 Pt 2):046117. Epub 2005/12/31. doi: 10.1103/PhysRevE.72.046117. PubMed PMID: 16383478.
3. Hilgetag CC, Burns GA, O'Neill MA, Scannell JW, Young MP. Anatomical connectivity defines the organization of clusters of cortical areas in the macaque monkey and the cat. Philos Trans R Soc Lond B Biol Sci. 2000;355(1393):91-110. Epub 2000/03/07. doi: 10.1098/rstb.2000.0551. PubMed PMID: 10703046; PubMed Central PMCID: PMCPMC1692723.
4. Goñi J, van den Heuvel MP, Avena-Koenigsberger A, Velez de Mendizabal N, Betzel RF, Griffa A, et al. Resting-brain functional connectivity predicted by analytic measures of network communication. Proc Natl Acad Sci U S A. 2014;111(2):833-8. Epub 2014/01/01. doi: 10.1073/pnas.1315529111. PubMed PMID: 24379387; PubMed Central PMCID: PMCPMC3896172.
5. Seguin C, van den Heuvel MP, Zalesky A. Navigation of brain networks. Proc Natl Acad Sci U S A. 2018;115(24):6297-302. Epub 2018/06/01. doi: 10.1073/pnas.1801351115. PubMed PMID: 29848631; PubMed Central PMCID: PMCPMC6004443.
6. Noh JD, Rieger H. Random walks on complex networks. Physical review letters. 2004;92(11):118701. Epub 2004/04/20. doi: 10.1103/PhysRevLett.92.118701. PubMed PMID: 15089179.
7. Lambiotte R, Sinatra R, Delvenne JC, Evans TS, Barahona M, Latora V. Flow graphs: interweaving dynamics and structure. Physical review E, Statistical, nonlinear, and soft matter physics. 2011;84(1 Pt 2):017102. Epub 2011/08/27. doi: 10.1103/PhysRevE.84.017102. PubMed PMID: 21867345.